AN EXPERIMENTAL INVESTIGATION INTO SPECIFIC HEAT OF NANOFLUIDS

A

THESIS

Submitted In Partial Fulfillment of the Requirement for the Award of Degree of

Master of Engineering

In

Thermal Engineering

Submitted by

TUSHAR ANAND

ROLL NO: 801183021

UNDER THE GUIDANCE OF

DR. S.S. MALLICK

(ASSISTANT PROFESSOR)

MECHANICAL ENGINEERING DEPARTMENT

THAPAR UNIVERSITY, PATIALA

CERTIFICATION

I hereby certify that the work which is being presented in on the topic "An experimental investigation into specific heat of nanofluids", in partial fulfillment of the requirements for the award of degree of Master of Engineering in Thermal engineering submitted in Mechanical Engineering Department of Thapar University, Patiala, is an authentic record of my own work carried out under the supervision of Dr. S.S. Mallick.

Date: 15/7/13
Place: PATIALA

Tushar Anand
(801183021)

This is to certify that the above statement made by the candidate is correct and true to the best of my knowledge.

15/7

Guide:
Dr. S.S. Mallick
Assistant Professor
Mechanical Engineering Department
Thapar University, Patiala

Countersigned by

Dr. Ajay Batish
Professor and Head
Mechanical Engineering Department
Thapar University, Patiala

Dr. S K Mahapatra
Senior Professor, Dean
Academic Affairs
Thapar University, Patiala

ACKNOWLEDGEMENT

No volume of words is enough to express my gratitude towards my guide, Dr. S.S. Mallick, Department of Mechanical Engineering, Thapar University, Patiala , who has been very concerned and has aided for all the material essential for the preparation of this report. He has helped me to explore this vast topic in an organized manner and provided me with all the ideas on how to work towards a research-oriented venture.

I would also like to thank, Dr Bonamali Pal, School of Chemistry and Biochemistry, Thapar University, Patiala, and Mr. Bhupinder Pal, Research Scholar, school of Chemistry and Biochemistry, Thapar university, Patiala, and my colleagues who were always there at the need of the hour and provided with all the help and facilities, which I required, for the completion of my dissertation.

Most importantly, I would like to thank my parents and the almighty for showing me the right direction out of the blue, to help me stay calm in the oddest of the times and keep moving even at times when there was no hope.

Tushar Anand

801183021

Thapar University, Patiala.

ABSTRACT

This dissertations presents an experimental investigation into the specific heat of nanofluids. Nanofluids, a term proposed by Choi in 1995 of the Argonne National Laboratory, U.S.A. in which nano-sized particles were suspended in liquids to design heat transfer fluids which has become necessary as the sizes of devices operating with increasing speeds as gone down to the micro level. Even at the mega level, power plant, large vehicles and nuclear fuel reactors pose a challenge due to heat transfer technology. While lot of research has been done on nanofluids, it is still inconclusive and there is no agreement on the findings between various research groups. Also, most of the research has been done in areas of improvement of thermal conductivity but it is very important to know its specific heat of nanofluid. The increased specific heat in coolants, lubricants, water increases the heat carrying capacity of the system and thus the different parameter like conductivity, viscosity is more effective. In the present work the specific heat of different nanoparticles – Silver, SWCNT, Zinc Oxide, Aluminium Oxide have been investigated. Set up for this is made whose accuracy is done by comparing it with deionized water (DI), Ethyl Glycol. Also, the effect of different temperature and varying size of nanoparticle have been investigated. The specific heat model is made by applying the data obtained from this experimental set up and is being validated with the previous data handbook and with that of the different nanofluid too. Model 2 of specific heat is more accurate than of model 2 when compared with the experimental value. Specific heat of nanofluid increases with the increase in temperature and decreases with with increase in volume fraction.

CONTENT **PAGE NO**

LIST OF FIGURES

CHAPTER 1: INTRODUCTION

1.1 Introduction

Nanofluids are new class of engineered fluid obtained by suspending nano-size **(**10^{-9} m) particles with average size below 100 nm in heat transfer fluids (Choi et al.1999). It can be thought as a mixture consisting of continuous base fluid component called "matrix" and a discontinuous solid component called "particles" mixed together by using the techniques known as ultrasonication and mechanical stirring (Das, Choi and Gallego, 2008). Oxides, metals, nitrides and non metals, such as carbon nanotubes are used as nanoparticles in nanofluids, while water, ethylene glycol, oils, and polymer solutions, conventional coolants are used as base fluids. The smaller size of nanofluids offer several advantages over conventional heat transfer fluids, such as long term stability, low abrasion, low pumping power, homogeneity and minimum clogging in flow passages (Gallego and Wang, 2002). These benefits make nanofluids potentially attractive to various industries having heat transfer applications such as microelectronics, transportation, biomedical, micro-fluids, nuclear, automobile, power generation, x-ray, refrigerators etc (Chandrasekar and Khanafer 2010). Miniaturized systems will reduce heat transfer fluid inventory, successful employment of nanofluid will result in significant energy and cost savings because heat exchange systems can be made smaller and lighter.

In spite of such merits and wide spread potential applications of nanofluids, nanofluid technology is still limited for commercial use because there is yet no proven standardized design process for accurately predicting important heat transfer properties, such as the nanofluids specific heat, thermal conductivity and viscosity because of the influence of various particle and fluid properties, such as the shape and size distribution of nanoparticles (Chon, 2004; Murshed, 2008; Mintsa, 2007; Teng, 2010) volume concentration of nanoparticles in base fluids (Wang, 1999; Li, 2006; Timofeeva, 2007) ultrasonication and storage time to prepare nanofluids (Timofeeva, 2007),

use of surfactants (Murshed, 2008; Li, 2006), pH value (Xie, 2002) and temperature (Murshed, 2008; Mintsa, 2007; Li, 2006; Das 2003), developing accurate fundamental model for the specific heat of nanofluids is a challenging task.

To meet potentially the increasing demand for high thermal conductive working fluids, (Zhou and Ni, 2008) focused on the basic thermophysical properties of nanofluids, for example, effective thermal conductivity, effective viscosity, thermal diffusivity, specific heat capacity, μCp/K for finding the convective heat transfer and flow characteristics of nanofluids. However, only thermal conductivity and little in viscosity are extensively covered in relevant papers (Bu-Xuan Wang et al. 2006). As a thermodynamic property, the specific heat capacity of a nanofluid dictates the nanoparticle and fluid temperature changes, which affect the temperature field of the nanofluid and hence the heat transfer and flow status. Other thermophysical properties, such as thermal diffusivity and prandtl μCp/K, Dittus and Boelter Correlation need the knowledge of specific heat capacity. Systems for utilizing low-temperature solar thermal energy include means for heat collection, usually heat storage, either short-term or interseasonal and distribution within a structure or a district heating network. The most important thing is to design such experimental set up which is cost effective and is easily available .

Hence, the purpose of this dissertation is to firstly Design/develop tester for measuring Cp. Secondly to carry out extensive experimental work to find out the effect of different particle size, volumetric concentration, sonication time, frequency on specific heat of different nanofluid. Thirdly to develop improved model for specific heat using the above experimental data obtained from new experimental set up.

CHAPTER 2: LITERATURE REVIEW

2.1 Synthesis of Nanofluids

Nanofluids are composed of solid nanoparticles dispersed in base fluid such as water, ethylene glycol, propylene glycol and so on. The advantages of nanofluids over the conventional heat transfer fluids had made it a emerging topic of research. Nanofluid is a mixture of nanoparticles in base fluids. There are two methods of formation of nano fluids, which are as follows:

1. Two Step Method (Das et al., 2006)
2. One Step Method (Das et al., 2006)

1. Two Step Method

In this method, dry nanoparticles are first produced, and then dispersed in a suitable liquid host. As nanoparticles have a high surface energy, aggregation and clustering are unavoidable which will result particles to clog and sediment at the bottom of the container. Therefore, making a homogeneous dispersion by two step method remains a challenge (Patel et al., 2006). However, there exist techniques to reduce this problem like high shear and ultrasound with these two methods. Nanofluids containing oxide particles are produced by this method. This method works well for oxide nanoparticles and is especially attractive for the industry due to its simple preparing method but its quickly agglomerated particles brings about many challenges. The two-step method is used where there is need of different concentrations for application. However, some surface treated (nanotube) nanoparticles showed excellent dispersion (Swanson et al. 2008). The first materials tried for nanofluids preparation were oxide particles, mainly because they are easy to make and chemically stable in solution (Das et al. 2006).

2. Single Step Technique

The single-step method is a process of combining the preparation of nanoparticles with the synthesis of nanofluids, for which the nanoparticles are directly prepared by physical vapour deposition (PVD) technique or a liquid chemical method (condensing nanophase powders from the vapor phase directly into a flowing low-vapor–pressure fluid is called VEROS). In this method drying, storage, transportation, and dispersion of nanoparticles are avoided, so the agglomeration of nanoparticles is minimized and the stability of the nanofluids is increased. A disadvantage of this method is that it is impossible to scale it up for great industrial functions and is applicable only for low vapour pressure host fluids (Keblinski et al., 2005, Goldstein et al., 2000, Wang et al., 2007). Recently, Chang et al., (2008) prepared nanofluids of TiO_2 nanoparticles dispersed in water by a one-step chemical method using a high pressure homogenizer.

2.2 Nanoparticles

A bulk material has constant physical properties regardless of its size, but at the nano-scale this is often not the case. Size-dependent properties are observed such as quantum confinement in semiconductor particles, surface plasmon resonance in some metal particles and superparamagnetism in magnetic materials. Nanoparticles are the particles with average size below 100 nm. Nanopaericles have superior mechanical, electrical, optical, magnetic and thermal properties than that of conventional bulk materials due to coarse grain structure (Das et al., 2007).

(i) Nanoparticle materials:

Nanoparticles which are used in nanofluids are made of different materials such as metals (Al, Cu, Ag, Au, Fe), metal oxides (Al_2O_3, CuO, TiO_2, WO_3, Fe_3O_4, ZnO), nitride ceramics (AlN, SiN), carbide ceramics (SiC, TiC), carbon nanotubes and composite materials such as nanoparticle core polymer shell composites or alloyed nanoparicles $Al_{70}Cu_{30}$ (Das et al, 20007; Choi, 1999; Yoo et al, 2007; Zhu et al, 2006;Yu et al., 2009).

(ii) Base fluids:

Water, oil and ethylene glycol are commonly used as base fluid (Das et al., 2007, Choi, 1999; Yoo et al., 2007; Timofeeva et al., 2007).

2.3 Applications of Nanofluids

Nanofluids are an exciting new category of more efficient heat transfer fluids that have the potential to greatly improve upon thermal management systems in a wide variety of applications, owing to their increased thermal conductivity and long term stability (Das et al., 2007, Choi, 1999; Yoo et al., 2007; Timofeeva et al., 2007). Some of the applications of nanofluids are as follows:

2.3.1 Cooling Applications

Crystal Silicon Mirror Cooling - One of the first applications of research in the field of nanofluids is for developing an advanced cooling technology to cool crystal silicon mirrors used in high

intensity x-ray sources. Lee and Choi et al, (1996) carried out analysis to estimate the performance of microchannel heat exchangers with water, liquid nitrogen, and nanofluids as the working fluid.

Electronics Cooling - Chien et al, (2003) were probably the first to show experimentally that the thermal performance of heat pipes can be enhanced by nearly a factor 2 when nanofluids are used. Water based nanofluids are used containing 17 nm gold nanoparticle as the working fluid in a disk shaped miniature heat pipe (DMHP). Then, measured the thermal resistance of the DMHP with both nanofluids and deionized (DI) water. The results show that thermal resistance of a DMHP is reduced significantly (40%) when nanofluids are used instead of DI water.

Vehicle cooling - Nanoparticles can be dispersed not only in coolants and engine oils, but in transmission fluids, gear oils, and other fluids and lubricants. These may provide better overall thermal management and better lubrication. Tzeng et al, (2005) were probably the first to apply nanofluid research in cooling a real-world automatic power transmission system. They dispersed CuO and Al2O3 nanoparticles into automatic transmission oil to investigate the optimum possible compositions of a nanofluid for higher heat transfer performance.

Transformer Cooling - The power generation industry is interested in transformer cooling application of nanofluids for reducing transformer size and weight. If the heat transfer capability of existing transformers can be increased, many of the upgrades may not be necessary. Xuan and Li Year and Yu et al, (2003) have demonstrated that the heat transfer properties of transformer oil can be improved by using nanoparticle additives.

Space and Nuclear Systems Cooling- You et al, (2004) have discovered the unprecedented

phenomenon that nanofluids can double or triple the CHF in pool boiling. Kim et al, (2004) found that the high surface wetability caused by nanoparticle deposition can explain this remarkable thermal property of nanofluid. The work is important in developing realistic predictive models of the CHF in nanofluids. The ability to greatly increase the CHF, the upper heat flux limit in nucleate boiling systems, is of paramount practical importance to ultra-high heat flux devices that use nucleate boiling, such as high power lasers and nuclear reactor components. Therefore nanofluids brought up exciting possibilities for raising chip power in electronic devices or simplifying cooling requirements for space applications.

2.3.2. Tribological Applications

Nanofluid technology develops better oil and lubricants. Recent nanofluid activity involves the use of nanoparticle in lubricants to enhance tribological properties of lubricants, such as load carrying capacity and antiwear and friction reducing properties between moving mechanical components. Que et al, (1997) performed experimentally in lubrication application and reported that surface modified nanoparticles stably dispersed in mineral oils are very effective in reducing wear and enhancing load carrying capacity.

2.3.3 Biomedical Applications

Nanofluids was originally developed primarily for thermal management application such as engine, microelectronics, and photonic. However, nanofluids can be formulated for a variety of other uses for faster cooling. Nanofluids are being developed for medical applications, including cancer

therapy. Jordan et al, (1999) suggested that iron based nanoparticles can be used as delivery vehicles for drugs or radiation without damaging healthy tissue by guiding the particles up the bloodstream to a tumor with magnets. In contrast to cooling, nanofluids could be used to produce higher temperatures around tumors, to kill cancerous cells without affecting nearby healthy cells. For most biomedical uses the magnetic nanoparticles should be below 15□nm in size and stably dispersed in water. A potential magnetic nanofluid that could be used for biomedical applications is one composed of FePt nanoparticles.

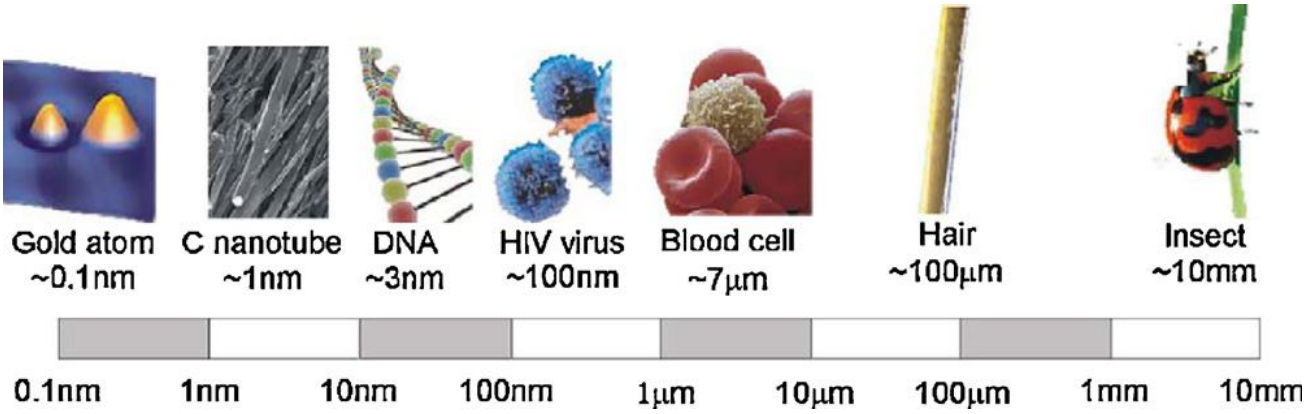

Figure 2.1: Length scale and some examples related (Serrano et al, 2009)

This FePt nanofluid possesses an intrinsic chemical stability and a higher saturation magnetization making it ideal for biomedical applications. However, before magnetic nanofluids can be used as drug delivery systems, more research must be conducted on the nanoparticles containing the actual drugs and the release mechanism.

2.4 Characterization Techniques

The need to characterize nanoparticles in solution before assessing the *in vitro* toxicity is a high priority. Particle size, size distribution, particle morphology, particle composition, surface area, surface chemistry, and particle reactivity in solution are important factors which need to be defined to accurately assess nanoparticle. Currently, there are no well-defined techniques for characterization of wet nanomaterials in aqueous or biological solutions.

(a) X-Ray Diffraction Analysis (XRD)

X-ray powder diffraction (XRD) is a rapid analytical technique primarily used for phase identification of a crystalline material and can provide information on unit cell dimensions**.** With the help of data base of known structure XRD is used for the phase identification and XRD is also used to determine crystal structure of unknown materials, strain, crystal size, orientation of single crystal or polycrystalline materials (Cullity and Stock 2001; Suryanarayana and Norton 1998; Waseda et al., 2001) explained the principle of operation of X-ray diffraction analysis, when X-rays are directed on the nanoparticle, electrons present in the material scatter the X-rays. Scattering results in maxima and minima of different intensity, if the material is crystalline. Bragg's law provides the conditions that must be satisfy for the reflected X-ray waves to be in phase with each other (constructive interference). If conditions of Bragg's law are not satisfied, destructive interference reduces the reflected intensity to zero. Bragg's law is $n'\lambda = 2D\sin\text{ø}$. Here λ is the X-ray wavelength, n is an integer, ø is the diffraction angle and D is the distance between crystal lattice planes. For each lattice spacing D, Bragg's law predicts a maximum at diffraction angle ø an X-ray diffraction pattern is obtained when the intensity of detected X-rays is plotted as a function of diffraction angle ø. To

identify the phase of tested sample XRD Pattern is matched with the pure substance. The plot obtained from XRD analysis shows the characteristic of the sample material.

(b) Dynamic Light Scattering (DLS)

Dynamic light scattering (also known as photon correlation spectroscopy or quasi-elastic light scattering) is a technique which determines the size distribution profile of nano particles in suspension solution. As Kaszuba et al, (2008) Dynamic light scattering (DLS) is a non-invasive technique for measuring the size of nanoparticles in a dispersion. The technique measures

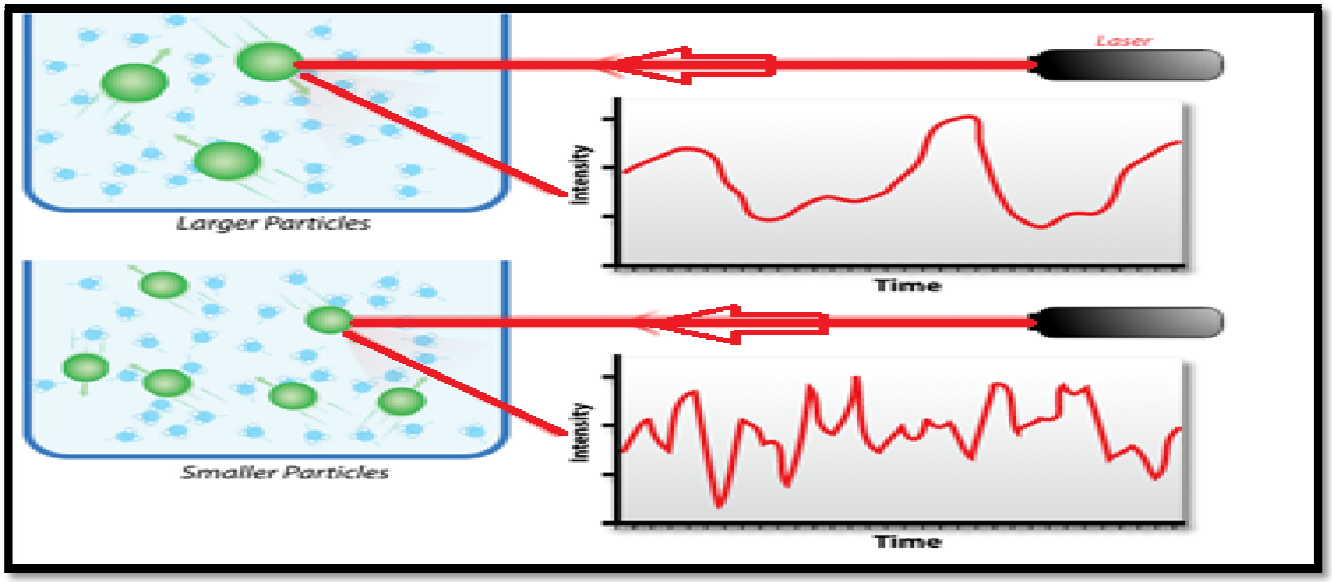

Figure 2.2: Diagrammatic view of the principle of SEM (Echlin et al, 2009)

the time-dependent fluctuations in the intensity of scattered light from a suspension of particles undergoing random, brownian motion. The lower size limit of the DLS technique depends on the amount of excess scattered light produced. This excess is the difference in scattering between the molecule or particle being studied and the dispersant it is prepared in. This in turn depends on a

number of factors such as the refractive indices of the molecule and dispersant, the concentration of the sample, the power and wavelength of the laser used, the sensitivity of them detector and the optical configuration of the instrument. When light hits small particles the light scatters in all direction so long as the particles are small compared to the wavelength (below 250 nm). Sample preparation either by filtration or centrifugation is critical to remove dust and artifacts from the solution. The dynamic information of the particles is derived from an autocorrelation of the intensity trace recorded during the experiment.

(c) Scanning Electron Microscope (SEM)

Scanning Electron Microscopy is a powerful method to investigate the surface structures of molicules. SEM is standardized method for imaging and the measuring the dimensions of nanometer and micrometer size particles because of high imaging speed and high resolution of SEM (Buhr et al., 2009). This technique provides a large depth of field. SEM has relatively wide range of magnification allows the investigator to easily focus in an area of interest on a specimen; an investigator may easily interpret SEM images (Stadtlander, 2007). Gabriel (1985) discussed about the operating conduction and operation of SEM: the basic operating condition for SEM involves high vacuum with minimum contagion, properly aligned column and saturated filament to its effective operating temperature. After setting the basic operating condition, for a given specimen the optimal imaging conditions are controlled by spot size, accelerating voltage and focus. Prepared specimen should be clean and conductive. Sometimes the filament is not heated until high vacuum is maintained. The alignment of column is evaluated, after filament has been saturated. Alignment of

electron gun is evaluated in reduced rapid or TV scan rate. In both the scanning mode, manipulate the gun X and Y electronic controls until uniform bright and centered image in CRT is obtained.

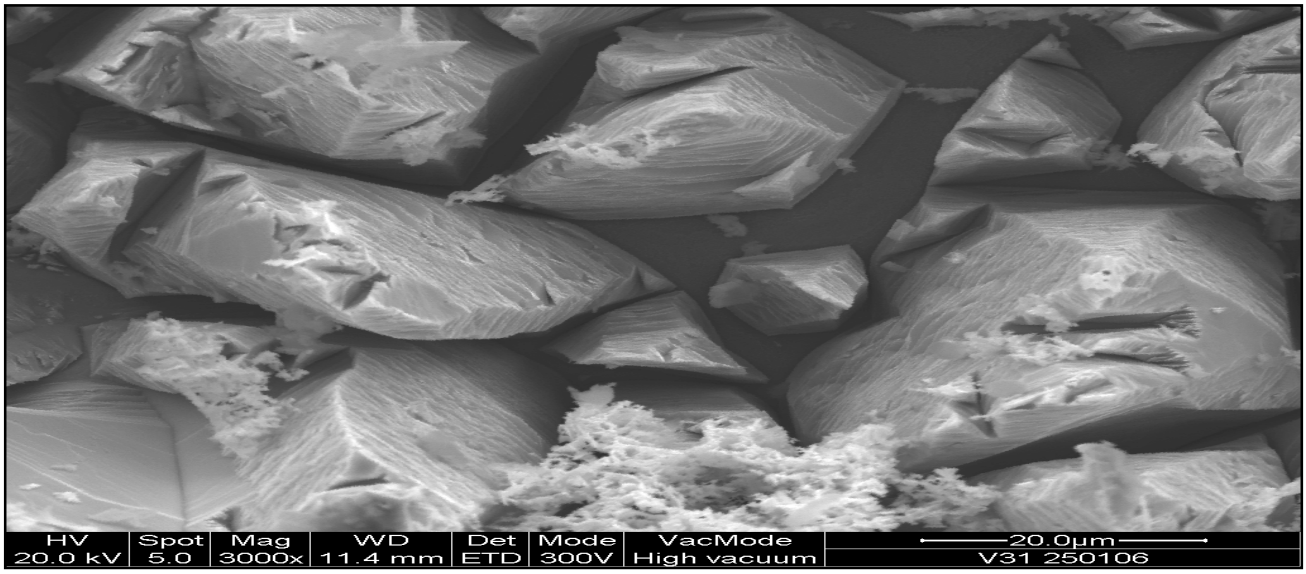

Figure 2.3: SEM view of SWCNT nanoparticle (Echlin et al, 2009)

Focus the image at about 1000X in rapid or TV mode. Select a view field where symmetrical object is able to be seen. If the image is not expanding symmetrically from its centre, correct its asymmetry by manipulating the stigmators. If the stigmator is not able to correct the asymmetry, the final aperture is off axis. Then again correct the stigmators by moving the aperture X and Y. After correcting the asymmetry, set the magnification and evaluate the specimen. A series of images from low to high magnification is obtained to examine the specimen. After finishing the examination, filament should be cooled for minimum 3 minutes before chamber is subjected to atmospheric pressure.

SEM is used for finding the shape and size of nanofluid

- Topography and morphology: For seeing the overall view of nanoparticle
- Crystallography: For seeing the crystal size and shape of nanoparticle.

- Orientation of grains: Viewing the different angles of the particle.

(d) Transmission Electron Microscope (TEM)

Transmission electron microscopy (TEM) is also a standardized method for imaging and measurements of dimension of nano and micro size structures due to their high imaging speed and high resolution (Buhr et al., 2009). The advantage of TEM over SEM is that the specimen's cellular structures can be viewed at extremely high magnifications (Stadtlander, 2007). Cullity and Stock (2001) explained the operation of TEM. TEM is a complex assembly of magnetic lenses, electron gun, a sample holder, several apertures and image viewing/ recording systems. Magnetic lenses are set into illuminating systems between sample and electron gun and those of imaging system after sample. There are three lenses in the imaging system and two condenser lenses in the illumination system. The traditional TEM mode adjusts condense lenses to illuminate the sample with approximately parallel beam. Beam covers sample area of several micrometer diameters at magnification lies between 20,000X and 100,000X. To control beam position or angle pre-specimen scanning or deflection coils are often used. In TEM to view the diffraction pattern, the intermediate lens is set to focus on the back focal plane of objective lens. In the case of viewing the image the intermediate lens is adjusted so that its object plane is plane of image of the objective lenses. If all the transmitted beams and diffraction beams were directed to combine in the first intermediate image plane, resultant images would be of little contrast.

2.5 Measurement of specific heat of Nanofluids

A heat-flux-type differential scanning calorimeter (TA Instruments Q2000) is used to measure the nanofluid specific heat capacities. The differential scanning calorimeter (DSC) measures the heat flux into a sample as a function of temperature during a user-prescribed heating regime. It accomplishes this by comparing the heat flux into a pan containing the sample with the heat flux into an empty pan.

2.5.1 Differential Scanning Calorimetry (DSC)

Introduction

DSC is a technique which is part of a group of techniques called Thermal Analysis. Thermal Analysis is based upon the detection of changes in the heat content (enthalpy) or the specific heat of a sample with temperature. As thermal energy is supplied to the sample its enthalpy increases and its temperature rises by an amount determined, for a given energy input, by the specific heat of the sample. The specific heat of a material changes slowly with temperature in a particular physical state, but alters discontinuously at a change of state. As well as increasing the sample temperature, the supply of thermal energy may induce physical or chemical processes in the sample, e.g. melting or decomposition, accompanied by a change in enthalpy, the latent heat of fusion, heat of reaction etc.

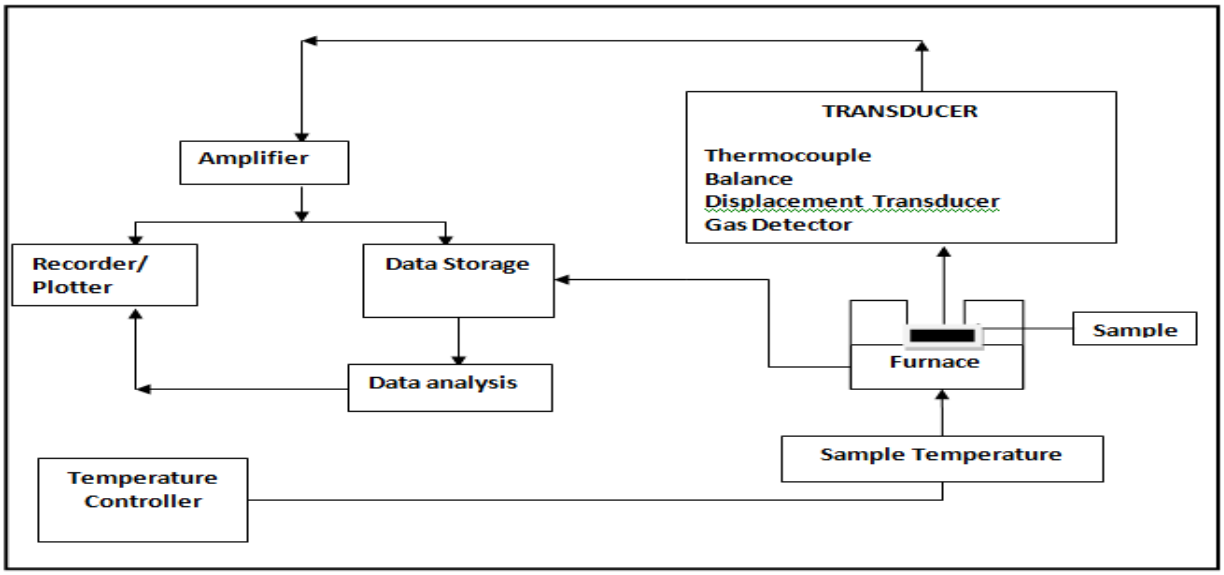

Figure 2.4: Schematic diagram of a modern thermal analyzer (Gill et al, 1984).

Such enthalpy changes may be detected by thermal analysis and related to the processes occurring in the sample .The transducer can be a thermocouple to measure heat flow (DSC or DTA), a balance to monitor weight changes (TG), or a linear variable differential transducer (LVDT) to detect changes in dimension (TMA). The transducer generates a voltage signal which is amplified, stored on magnetic tape or disk along with a direct temperature response from the sample, and recorded on a printer/plotter.

Theory

Differential scanning calorimetry (DSC) is mainly used at the Molecular Energetic Group for the determination of temperatures and enthalpies of phase transitions (solid-liquid or solid-solid) and thermal decompositions (e.g. dehydrations), and heat capacities of solids and liquids.

Physical and chemical changes may often be induced by raising or lowering the temperature of a substance. Typical examples are phase transitions, such as fusion, or chemical reactions, such as the

dehydration of a solid hydrate. Differential scanning calorimetry (DSC) was designed to obtain the enthalpy and temperature of those processes, and also to measure temperature-dependent properties of substances, such as the heat capacity. This is done by monitoring the differential heat flow rate to a sample (S) and to reference cell (R):

$$\Delta\emptyset = \emptyset_S - \emptyset_R = (dQ/dt)_S - (dQ/dt)_R \quad (1)$$

The temperature is usually increased or decreased linearly at a predetermined rate but isothermal experiments can also be performed. In some cases DSC experiments may provide kinetic data.Two general types of DSC apparatus, which differ on the operation principle, are available: heat flux DSC and power compensation DSC. The equipment used at the Molecular Energetics group is a power compensation DSC 7 from Perkin Elmer (Figure 2.4). In a heat flux DSC, the temperature difference between the sample S and the reference R is recorded and converted to a difference in heat flow rate to the sample and to the reference, using a suitable calibration factor. In a power compensation DSC (Figure 2.4) the sample and the reference crucible holders consist of two small furnaces, $\mathbf{1_S}$ and $\mathbf{1_R}$, each one equipped with a temperature sensor, $\mathbf{2_S}$ or $\mathbf{2_R}$, and a heat source, $\mathbf{3_S}$ or $\mathbf{3_R}$. The furnaces are located inside a cell **4** whose temperature is not monitored. The system of furnaces is controlled by two separate loops, one for average temperature control and the other for differential temperature control. The average temperature control loop ensures that the average of the sample and reference temperatures is increased at a programmed rate β. If the sample undergoes an endothermic or exothermic transformation, or a heat capacity change, a temperature difference, ΔT, will tend to develop between $\mathbf{1_S}$ and $\mathbf{1_R}$. The differential control loop automatically adjusts the power supplied to each furnace, so that ΔT is maintained as close to zero as possible during an experiment (the value of ΔT is actually never zero because the working principle of the control system is based on the

existence of a small error signal). The recorded output signal of the calorimeter is proportional to the differential heat flow rate, ΔΦ, between the sample and the reference. In the case of fusion, for example, the overall ΔΦ vs tdifference will be detected as a peak in the measuring curve, whose onset gives the temperature of fusion of the sample and the area is proportional to the corresponding enthalpy of fusion.

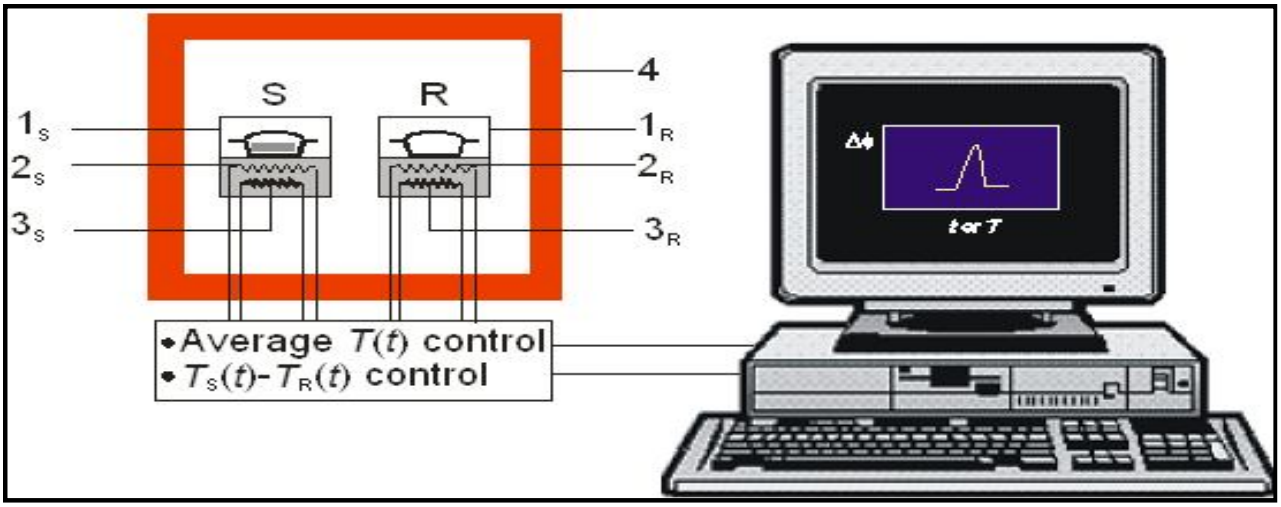

Figure 2.5: Calorimeter control circuits (Gill et al, 1984).

The molar enthalpy of fusion, $\Delta_{fus}H_m$, is calculated from :

– (2)

where m and M are the mass and the molar mass of the sample, respectively, A is the area of the experimental curve, and ε is the energy equivalent of the calorimeter. The value of ε is obtained by calibration. The most widely recommended calibration method involves the determination of the enthalpy of fusion of one or more standard substances (e.g. indium). These studies also allow the calibration of the temperature scale of the instrument based on the observed temperature of fusion

onsets. The enthalpy of fusion given by equation (2) strictly refers to a non-isothermal process such as:

$$A(s, Ti) \rightarrow A(l, Tf) \qquad (3)$$

where Ti and Tf represent the initial and final temperature of the peak. Normally the differenceTf-Ti is not very large. In this case it is generally a good approximation to assume that the experimentally obtained $\Delta_{fus}H_m$ value refers to an isothermal process occurring at the onset temperature of the process. Nevertheless, the calculation of the enthalpy of the fusion process under isothermal conditions from $\Delta_{fus}H_m$ can be performed as described . The determination of the heat capacity as a function of the temperature usually involves three consecutive measurements

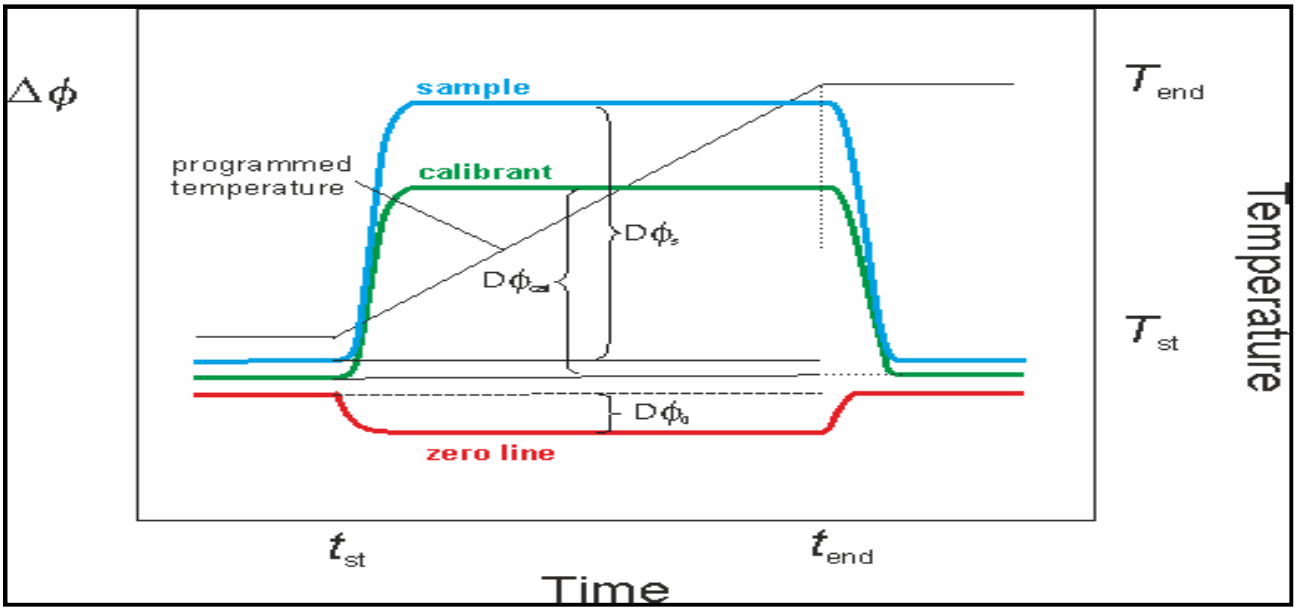

Figure 2.6: DSC measuring curves for the determination of heat capacities. (Gill et al, 1984)

First, the zero line is recorded using two empty crucibles. Next, a calibrant substance (usually alumina, i.e. synthetic sapphire) is placed in the sample crucible and the temperature program is

repeated. Finally, the calibrant is replaced by the sample under study (keeping the crucible) and the temperature program run a third time. The ordinate difference between the traces of the calibrant curve and of the zero line obtained for a given time t leads to the scorresponding value of ∈:

$$\in_{\emptyset} = \frac{\beta C_p(cal)}{\Delta\emptyset_{cal} - \Delta\emptyset_0} \quad (4)$$

where Cp (cal) represents the heat capacity of the calibrant. Once the variation of K_Φ with the time and, consequently, with the temperature, is known, the heat capacity of the sample, Cp(cal), can be derived from the difference between the traces of the sample curve and the zero line:

$$C_p(S) = \frac{\in_{\emptyset}(\Delta\emptyset_S - \Delta\emptyset_0)}{\beta} \quad (5)$$

The samples are enclosed in crucibles, which may or may not be hermetically sealed, and exist in a variety of shapes, depending on the type of apparatus and application. Crucibles are usually made of high thermal conductivity materials and aluminum is by far the most widely used. As illustrated in Figure 2, the reference normally consists of an empty crucible identical to the sample crucible. During the experiments, a purging gas (e.g. helium, argon, nitrogen) is flowed through the cell at a constant rate to ensure that the atmospheric conditions are as uniform as possible in all experiments.

2.6 Experimental Investigation Carried out By Other Researchers

Various researchers have done work on the specific heat measurement of nano fluids. These researchers have done experiments on different combinations of nanoparticles and fluids combinations. Based on the research work they had some results. So the work by various researchers is as follows:

Bu-Xuan Wang et al, (2006) Studied the different contributions of surface and interior atoms to the specific heat capacity of a nanoparticle and calculated the specific heat capacity of a nanoparticle with the Einstein and Debye models, to study the size and surface effects on the specific heat capacity, while using the elastic continuum assumption. The effect of size and temperature and the softening of surface atom vibrations were studied, and a new dimensionless variable was proposed to characterize the effect of particle size and temperature on the specific heat capacity. The proposed model was used to fit experimental data for CuO nanoparticles. It shows that this model fits well with related experimental data.

Donghyun Shin et al, (2007) The specific heat data of the eutectic of lithium carbonate and potassium carbonate 62:38 along with their silica doped nanofluid at concentration of 1% by weight have been presented in this study. Accounting for the measurement uncertainties, the specific heat of the nanofluid was enhanced by 25% compared with that of the pure eutectic. The stability of the high temperature nanofluids was also verified by using electron microscopy SEM and TEM after repeated thermocycling and melting/ solidification. The microscopy results showed that the nanofluids were fairly stable with the minimal agglomeration of the nanoparticles after repeated thermocycling. A

percolation network of a higher density eutectic material surrounding the nanoparticles was also observed in these microscopy images. This result is contrary to a previous study in the literature, which showed a decrease in the specific heat of the nanofluid possibly due to the agglomeration and precipitation of the particles in the mixture which was not verified. The anomalous enhancement on the specific heat for the high temperature nanofluid samples can be potentially due to the high specific surface energy of the nanoparticles. In this the anomalous enhancement of specific heat capacity of high-temperature Nanofluids was seen. Alkali metal chloride salt eutectics were doped with silica nanoparticles at 1% mass concentration. The specific heat capacity of the nanofluid was enhanced by 14.5%. Dispersion behavior of the nanoparticles in the eutectic was confirmed by scanning electron microscopy (SEM). Three independent competing transport mechanisms are enumerated to explain this anomalous behavior.

Le-Ping Zhou et al, (2009) The specific heat capacity of nanofluid made by ethylene glycol and copper dioxide nanoparticle inclusions, measured at room temperature, were compared with two kinds of models for determination of the specific heat capacity of nanofluid. The particle size effect and particle-liquid interface effect on the specific heat capacity of nanofluid are also discussed briefly. The effect of liquid adsorption on suspended nanoparticles' surface will also increase the specific heat capacity of nanofluid to some extent with increasing nanoparticles' volume concentration, which may be worthy to be investigated further for nanofluids.

Donghyun Shin et al, (2011) studied the specific heat capacity of neat chloride eutectics and their nanofluids obtained by doping with SiO_2 nanoparticles (at 1% weight concentration) with 20–30 nm nominal diameter were explored in this. The SiO_2 nanofluid enhanced the specific heat capacity by

14.5% compared with that of the neat chloride salt eutectic. This enhancement is significantly higher than the measurement uncertainty of 2–4%. Three independent thermal transport mechanisms were proposed to explain the unusual enhancement of the specific heat capacity: (1) Mode I: enhanced specific heat capacity of nanoparticle due to higher specific surface energy (compared with bulk material); (2) Mode II: additional thermal storage mechanisms due to interfacial interactions (e.g., such as interfacial thermal resistance and capacitance) between nanoparticle and the adhering liquid molecules due to the extremely high specific surface area of the nanoparticle; and (3) Mode III: the existence of semi-solid liquid layer adhering to the nanoparticles, which are likely to have enhanced specific heat capacity due to the smaller inter-molecular spacing similar to the nanoparticle lattice structure on the surface (compared to the higher inter-molecular spacing in the bulk liquid).

Murshed et al, (2012) studied the effective specific heats of the nanofluids are found to decrease significantly with increasing volume fraction of nanoparticles. Besides particle volume fraction and particle materials, particle shape and type of base fluid also play important roles in alteration of these thermal properties of nanofluids.The effective specific heats of nanofluids calculated from the volume fraction mixture rule-based correlation are found to agree fairly well (within 7%) with experimental results.

Le-Ping Zhou et al (2007) shows that the specific heat capacities of nanofluids are different from that of base fluid and vary with the size and volume concentration of nanoparticles. The specific heat capacity of CuO nanofluid decreases gradually with increasing volume concentration of nanoparticles. In most of the cases, however, there are no experimental data available for specific heat capacity, such that two kinds of models have been generally adopted to deduce it from the value

of base fluid and nanoparticles. One is macroscopic, that the specific heat capacity of a nanofluid is equal to the volume average of the specific heat capacities of base fluid and nanoparticles. The other is microscopic, which assumes the base fluid and the nanoparticles are in their thermal equilibrium, respectively. Using the volumetric heat capacity instead, the volumetric heat capacity of a nanofluid can be expressed as the sum of the volumetric heat capacities for base fluid and nanoparticles, using their respective volume concentrations.

CHAPTER 3: EVALUATION OF EXISTING MODELS

3.1 Existing Models of Specific Heat

There are two specific heat models widely used in the nanofluid literature. Model I is similar to mixing theory for ideal gas mixtures (Cho et al, 1998). This is macroscopic, that is, the specific heat capacity of a nanofluid is equal to the volume average of the specific heat capacities of base fluid and nanoparticles.

$$C_{pnf} = (1-\phi)C_{fs} + \phi C_{pbf} \tag{3.1}$$

Model II (Murshed et al., 2006 and Venerus et al., 2006) is based on the assumption of thermal equilibrium between the particles and the surrounding fluid. The is microscopic, which assumes the base fluid and the nanoparticles are in their thermal equilibrium. The nanofluid specific heat capacity per unit mass of nanofluid, that is, the nanofluid specific heat is

$$C_{nf} = \frac{\left(C_{ps}\phi\rho_s + C_{pbf}(1-\phi)\rho_{bf}\right)}{\rho_{nf}} \tag{3.2}$$

where ρ_s is the density of the solid nanoparticle, ρ_{bf} is the density of the base fluid, and ρ_{nf} is the density of the nanofluid. The product of density and specific heat is the volumetric heat capacity of each constituent and that of the nanofluid.

Models given in the equations are being compared with the experimental data for the same range of volume fraction, temperature and particle size. Lines of best fit have been drawn through the experimental data to indicate their trends. The following parameters are considered for the purpose of calculation in this paper:

(a) Specific heat and density of water are as 4.186 kJ/kgK and 1000 kg/m^3, respectively;

(b) Density of Al_2O_3 particles were as mentioned in their respective references, such as ρ_p: 3965 kg/m^3

(c) Specific heat of Al_2O_3 is 880 J/kg K;

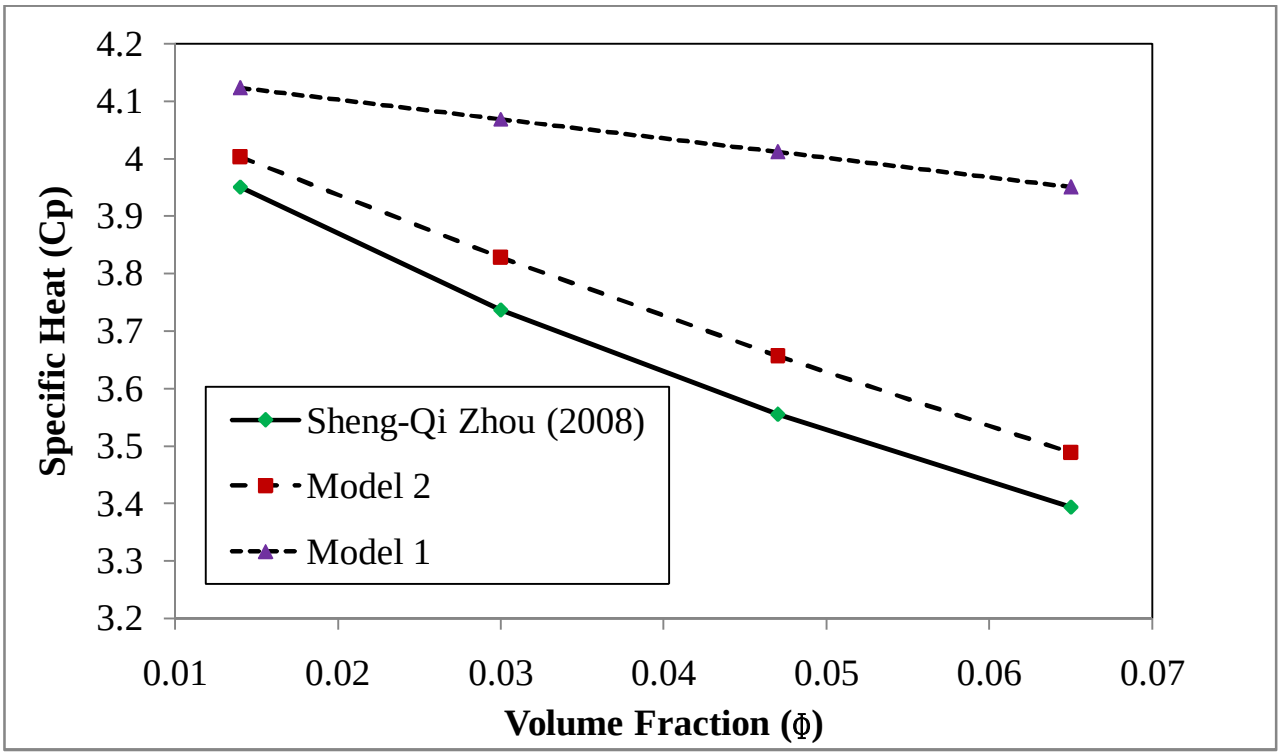

Figure 1: Experimental versus predicted values of specific heat with increase in volume fraction of Al_2O_3 nanoparticles, d: 50 nm, T: 35^oC

Figure 1 shows that all the theoretical models over the experimental data. With increase in nanoparticle volume fraction, the predicted values increase for all the models, also the amount of

inaccuracy increases. One reason for the model predictions to be not matching with the experimental data could be due to models mainly assume particles are non-clustering type (i.e. all the particles have separate identity within the nanofluid volume) and use simplified particle dimension (such as nominal diameter of nanoparticles), whereas the nanoparticles may actually be present in cluster form.

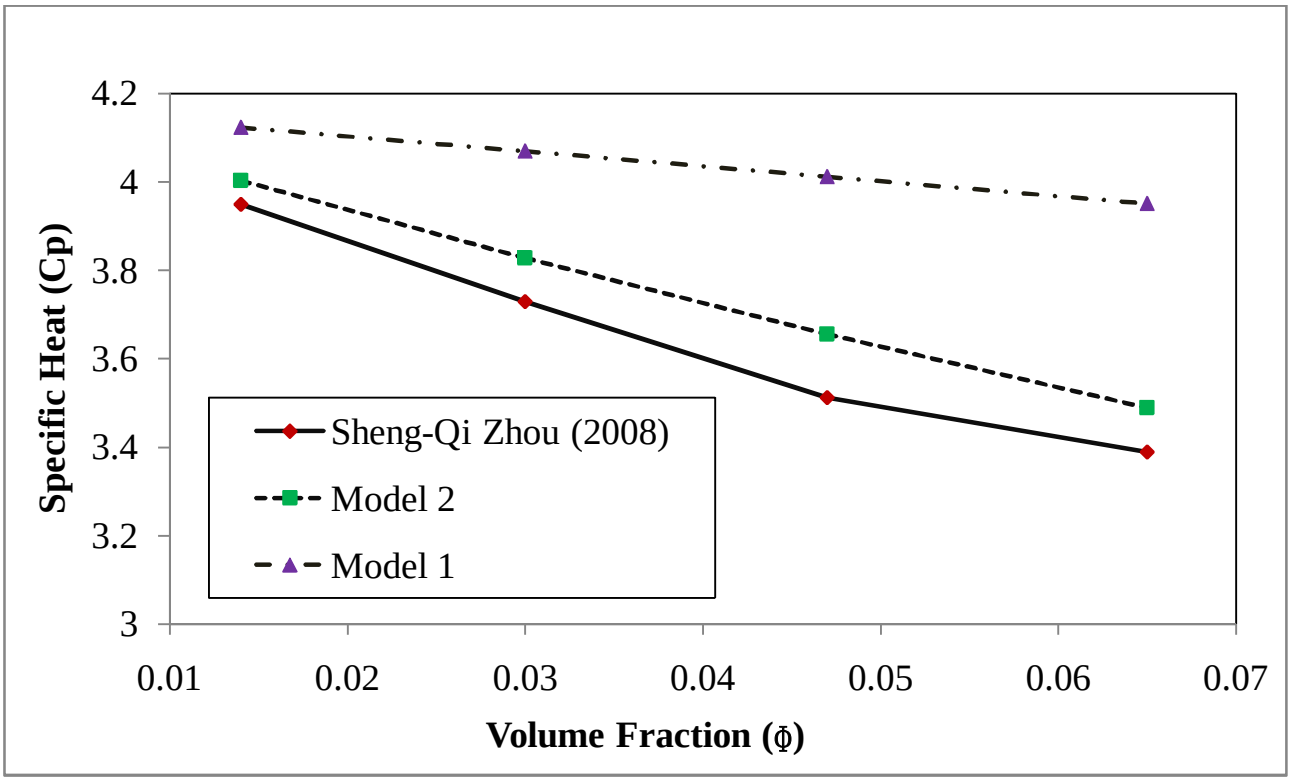

Figure 2: Experimental versus predicted values of specific heat with increase in volume fraction of Al_2O_3 nanoparticles, d: 50 nm, T: 45^oC

In Figure 2, experimental data of nanofluid specific heat with nanoparticle diameter of 50 nm, 45^oC temperature and for a range of volume fraction were compared with theoretical model.

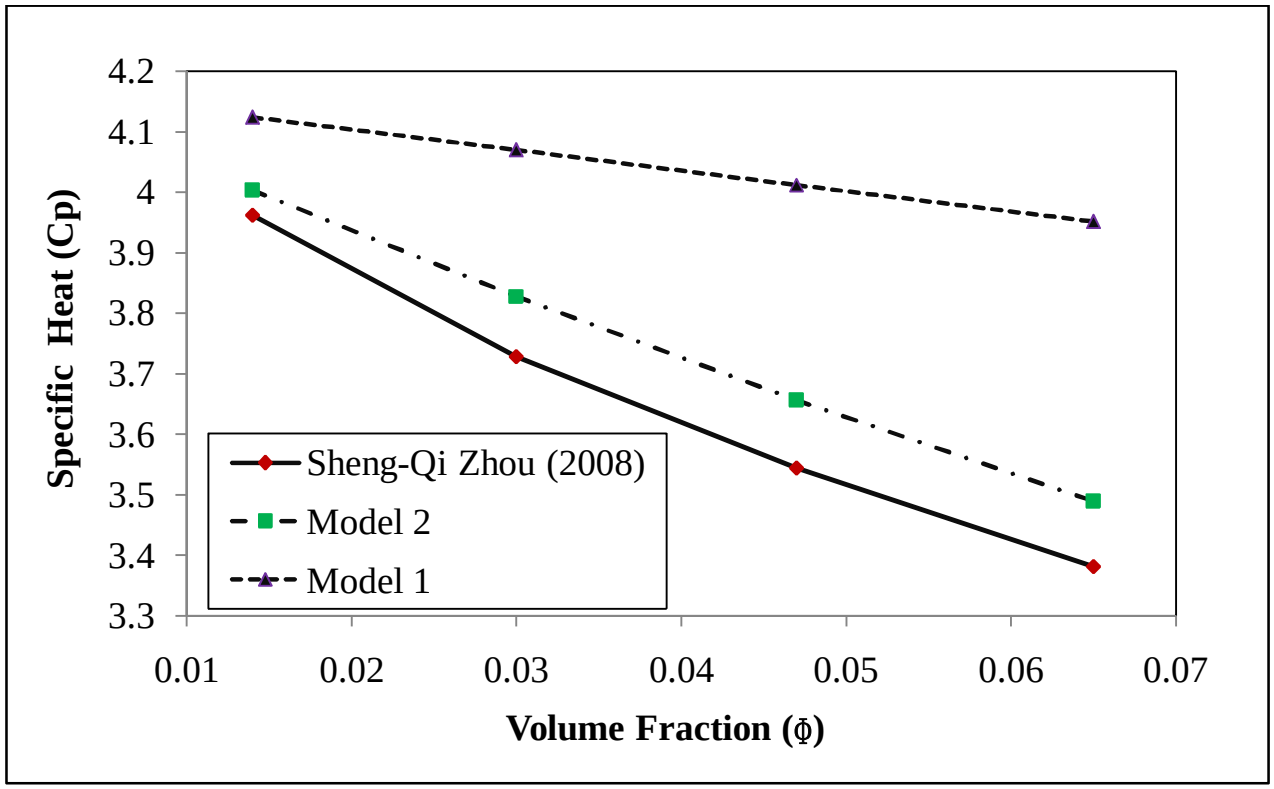

Figure 3: Experimental versus predicted values of specific heat with increase in volume fraction of Al_2O_3 nanoparticles, d: 50 nm, T: 55^oC

CHAPTER 4: DESIGN AND FABRICATION OF EXPERIMENTAL SET-UP FOR SPECIFIC HEAT OF NANOFLUID

4.1 Experimental Setup and Procedure

The experimental setup for measuring the specific heat of any liquid is shown in Fig. 4.1. The apparatus consists of a 20cm long and 7cm inside borosilicate container. This low thermal conductivity and low diffusivity material is selected to minimize heat flow from the fluid into the container wall and to ensure that the major portion of heat goes into the fluid to increase its temperature. The apparatus is designed to hold about 900 ml of liquid. The nanofluids are heated from about 298K to 323K by using an electrical immersion heater, as shown in Fig. 4. Ten copper-Constantan thermocouples are placed in the apparatus. Four thermocouples are placed within the liquid volume; one at the top, one at the bottom, and two in the middle ,one on the heating coil. The average of the four temperatures in the liquid is taken as the mean temperature. Two thermocouple is placed on the outer surface of the container and two on the outer surface of second insulation and one at the midpoint of the last insulation. These thermocouples are connected to a data logger that records the temperature data at every 5 min interval. The container is insulated by two layers of insulation. The inner layer is 7.1 cm thick fiber glass insulation surrounding the container that fits the contour of the cylindrical container. The outer layer consists of 10 cm thick extruded polystyrene board insulation. This arrangement minimizes the heat flow away from the fluid. A Variac is used to supply constant wattage to the immersion heater, and the power input into the nanofluid is monitored by a power meter. The thermal energy supplied to the electrical heater heats the nanofluid, heating coil, container, and the insulation. Each of these components was weighed carefully in a mass balance. A small amount of heat is also transmitted to the environment through the insulation. The specific heat of a nanofluid was calculated from the following equation:

$$C_{P_{nf}} = \frac{\dot{Q}\Delta t - m_C C_{PC} \Delta T_C - m_{co} C_{PCO} \Delta T_{CO} - m_{in} C_{PIN} - \dot{q}_L \Delta t}{m_{nf} \Delta T_{nf}} \quad (6)$$

where Q is the heat applied to the electrical heater in watts determined from the power meter. The time interval t is measured by the data logger s, T is the temperature rise K, m is the mass in kg, Cp is the specific heat J /kg K, and $\dot{q}_L$ is the heat transfer to the environment (W). The subscripts C represents the container, CO the heating coil, and IN the insulation. The masses of the container, coil, and insulation are measured individually by an electronic mass balance. The specific heat of container borosilicate glass is taken from a handbook, and the specific heats of the coil and insulations are taken from Incropera, F. P et al (1996).

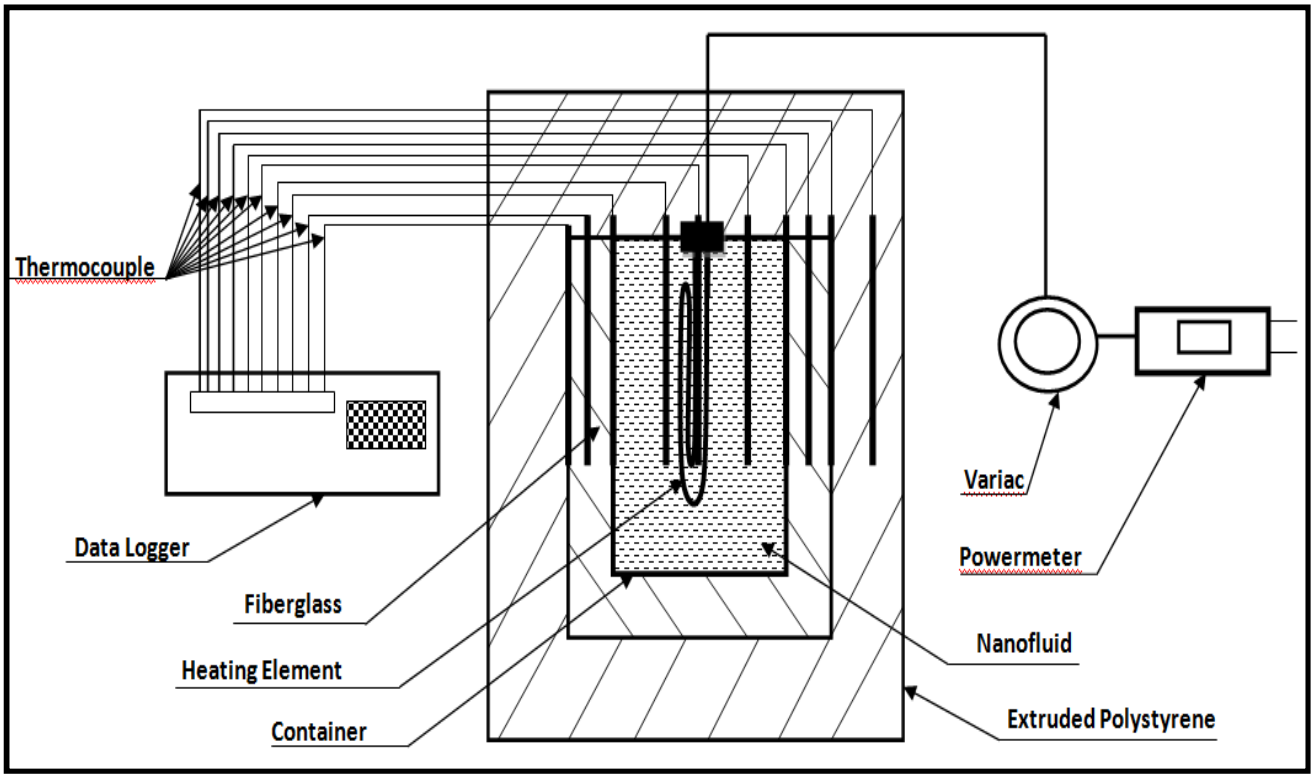

Figure 4.1: Layout of Experimental Set Up For Specific Heat

The temperature change T is recorded at every 15 s interval. The surface temperatures of the insulations and their dimensions are measured at the same time interval. The thermal conductivities of insulations are taken from Incropera, F. P et al (1996). Using these data the heat transfer to the environment through the insulation is calculated from the heat conduction equation.

2.5.3 Components of Experimental Setup

1. Borosilicate Container

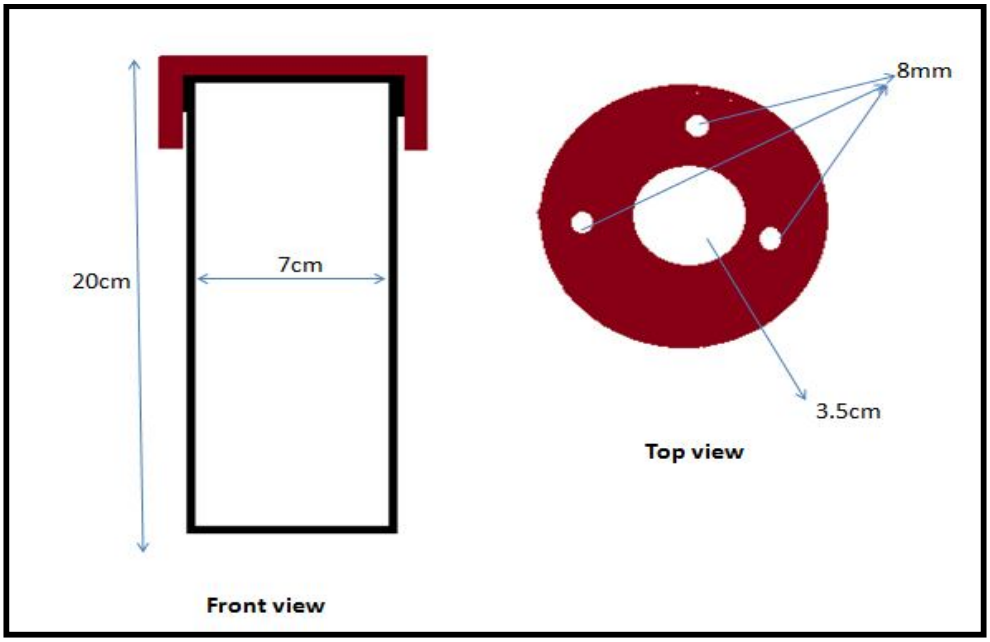

Figure 4.2

Table 1. Physical And Chemical Properties

Height	20cm
Specific Heat	1500J/KgK
Thickness	1cm
Internal Diameter	7cm
Material	Borosilicate
Weight	445.20gm
Conductivity	1.14W/mK

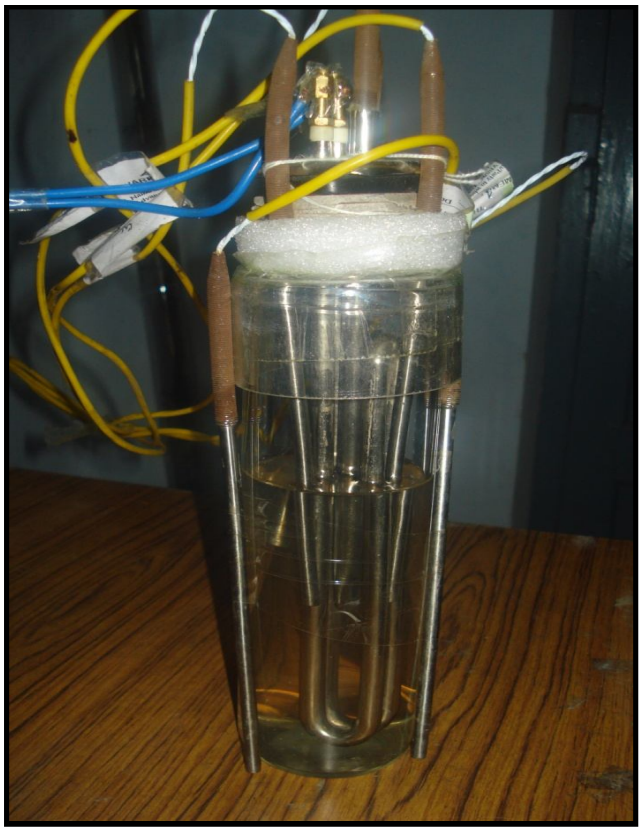

Figure 4.3

2. Data Logger

Figure 4.4

Table 2. Technical Specifications

Casing	Polycabornate, watertight to IP68 Humidity loggers splash proof from top
Weight	500 g
Resolution	Temperature: Better than 0.1°C (see sensor specifications)Humidity: Better than 0.1%RH
Size	65 × 31 × 106 mm
Ambient	-40 + 85°C
Sensor	Temperature: Precision Thermistor or Pt100

3. Dimmerset (Variac)

- Rated for 240V A.C. 50/60Hz. single phase supply and three phase model for 415V A.C. 50/60Hz three phase 4 wire supply.

- The output voltage of these Toroidal or variable transformer can be varied smoothly over two ranges:
    - Zero to full supply voltage
    - Zero to approx. 12% higher than the supply

Figure 4.5

4. Fiberglass

Figure 4.6

Table 3. Physical And Chemical Properties

Height	30cm	Conductivity	1.14W/mK
Internal Diameter	7cm	Material	Glasswool
Outer Diameter	13.5cm	Weight	445.20gm
Thickness	6.5cm	Specific Heat	1500J/Kg

5. Heating Element

Figure 4.7

Table 4. Specification

Weight	270.97gm
Specific heat	448J/KgK
Material	Stainless Steel

Ansys View of Heating Coil With Container And Four Thermocouples.

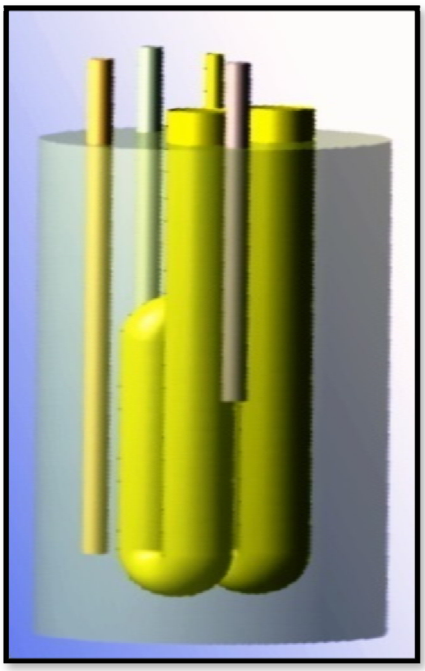

Figure 4.8

Ansys View of Heating Coil with Container, Thermocouple and its cap.

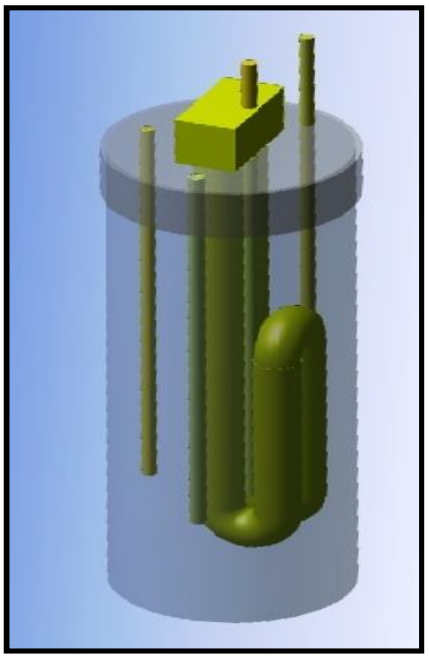

Figure 4.9

6. Extruded Foam

Figure 4.10

Table 5. Specifications

Weight	579.25gm
Specific Heat	1.309KJ/KgK
Conductivity	0.29W/mK

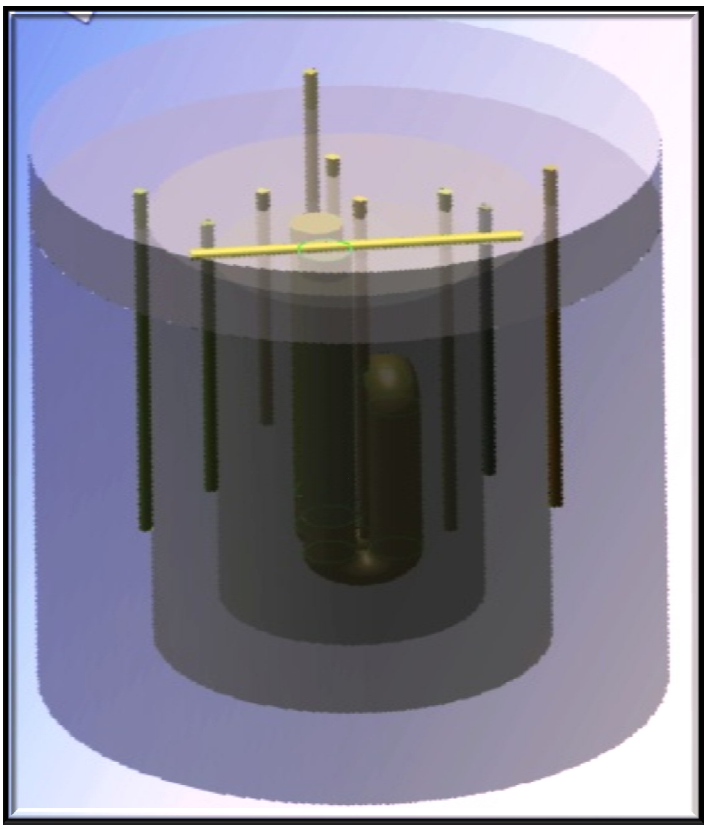

Ansys view to show exact location of insulation (extruded foam, glasswool) heating coil, and thermocouple

Figure 4.11

7. Thermocouples

Table 6. Specifications

Thermocouple	10
Material	Copper
Length	10cm
Thickness	7mm

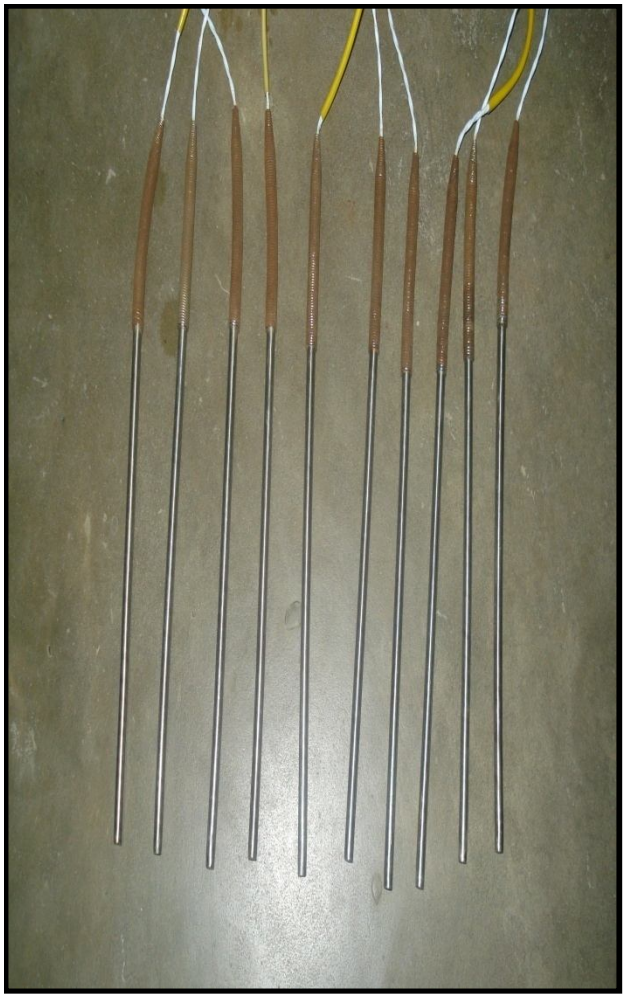

Figure 4.12

8. Ammemeter

Figure 4.13

Specifications

Standards: IEC 51, BS 89

Overload : CURRENT-1.2 x rating x VOLTAGE-1.2 x rating for 210 x r- 2 x rating for 5 secs.ating for 5 secs.

Table 7. Specifications

Accuracy	Class 1.5
Dimensions	48x48mm
Ratings	100-125v
Scale	0-150v

9. Voltmeter

Figure 4.14

4.2 Calibration Of Experimental Set Up

After the fabrication of set up , it is being calibrated by the help of the known data of water and ethyl glycol from data handbook of ashrae . in this T1, T2, T3, T4, T5, T6, T7, T8, T9, T10, T11 are the thermocouple attached to the setup at different places to accurately measure the temperature at different point . in this T1,T2 are at the outer surface of the container, T3 at the heater, T5, T4, T6 in the container to record the temperature of the nanofluid, T7, T8 at the outer of glass wool of the first insulation T9 to record the temperature of the extruded foam and T10 at the top surface of the container to record the lost temperature. Here the average of the temperature T4, T5, T6 is the temperature recored of that of the nanofluid. After putting the thermocouple at different place the temperature is recorded of that of the water and ethyl glycol at different concentration.Following are the data for the water and that of the ethyl glycol which are as follows:

TABLE 4.1: Specific heat of DI water

T (min)	V	I	T1	T2	T3	T4	T5	T6	T7	T8	T9	T10	T11	Varia c	Specif ic Heat(Cp)
5	0	0	22.9	21.9	23.9	23	23.8	21.5	23.4	23.8	23.6	24.3	25	0	
5	21	0.79	23.2	22.3	26.5	24.8	25.8	23.9	23.6	23.8	24	24.4	25	22	4.06
5	27	1	27.8	27.3	35.8	33.5	34.7	32.6	24.2	24.3	24.3	24.9	25.2	24	3.99
5	35	1.32	34.9	34.2	43.1	40.6	41.6	41.9	39.8	26	26.3	25.5	26.8	25	4.16
5	40	1.52	36.8	36.4	49.8	46.9	48.4	46.4	26.3	26.8	27.3	27	27.7	27	4.17
5	45	1.70	42.4	42.3	58.5	55	56.4	54.4	26.5	26.6	26.1	27.6	27.5	29	4.2

TABLE 4.2: Specific heat of Ethyl Glycol (25%)

T (min)	V	I	T1	T2	T3	T4	T5	T6	T7	T8	T9	T10	T11	Varia c	Specif ic Heat(Cp)
5	1	-0.01	22.3	20.9	23.3	22.2	23.1	21.1	23.3	23.4	23.6	23.9	24	0	3.5
5	26	0.98	22.6	21.6	28.4	25.3	26.9	23.5	23.5	23.6	23.8	23.9	23.8	22	3.2
5	36	1.36	24.4	23.3	35.3	30.9	33.6	29.4	23.6	23.6	24	24.3	24	24	3.8
5	50	1.88	29.1	27.9	49	40.9	44.9	38.6	23.8	23.9	24.1	24.9	25	25	3.7
5	60	2.26	34.8	34.1	65.5	56.1	61.9	54.2	24.4	24.3	24.9	24.9	25.1	27	3.8
5	70	2.65	51.5	49.8	83.8	74	79.4	71.1	25.3	25.3	25.2	39.9	30	29	3.9

TABLE 4.3: Specific heat of Ethyl Glycol (30%)

T (min)	V	I	T1	T2	T3	T4	T5	T6	T7	T8	T9	T10	T11	Varia c	Specif ic Heat(Cp)
5	0	0	24.3	23.3	25.2	24.2	25.1	22.9	25.3	25.3	25.6	25.9	27	0	
5	24	0.92	24.5	23.4	28.4	26.9	27.9	25.7	25.4	25.4	25.8	26.1	27.1	22	4.23
5	25	0.95	26	25.2	30.9	29.4	30.4	28.4	25.5	25.4	25.9	26.2	27.2	24	4.27
5	35	1.35	33.5	36.2	50.3	47.5	49	46.9	27.1	26.6	26.8	28.5	28.9	25	4.18
5	40	1.52	36.3	36.2	50.2	47.5	49	46.9	27.1	26.6	26.8	28.5	28.9	27	4.6
5	46	1.76	43.4	43.4	60.1	56.2	58.2	55.9	27.3	27	27.1	29.5	30	29	4.5

TABLE 4.3: Specific heat of Ethyl Glycol (50%)

T (min)	V	I	T1	T2	T3	T4	T5	T6	T7	T8	T9	T10	T11	Varia c	Specif ic Heat(Cp)
5	0	0	25	23.3	25.4	24.4	25.2	23.3	26.4	26.4	26.4	26	27.5	0	
5	22	0.84	25.1	23.5	28.4	26.9	27.7	26.3	26.4	26.4	26.4	26.6	27.5	22	3.12
5	24	0.90	25.8	24	29.9	29	29.9	27.6	26.8	26.5	26.6	26.9	27.5	24	3.2
5	29	1.09	31.8	29.9	40.6	38.8	39.8	36.9	28.1	27.9	27.3	27.8	28.5	25	3.3
5	32	1.23	32.9	30.9	42.9	41.1	42.3	42	30.1	28.5	27.6	28.3	29	27	3.4
5	37	1.41	36.3	34	48.9	47	48	45	29.4	28.9	27.9	28.9	29	29	3.6

The specific heat obtained from new experimental set up is being validated by the specific heat value from that of the existence hand book of ASHRAE (1994) to know the accuracy of the set up. This is being done for different base fluid and that of the nanofluid too with different temperature and with different size of the nanoparticle Incropera et al, (1996). Data were taken from different data hand book to validate from different angle the specific heat of that obtained from new experimental set up.

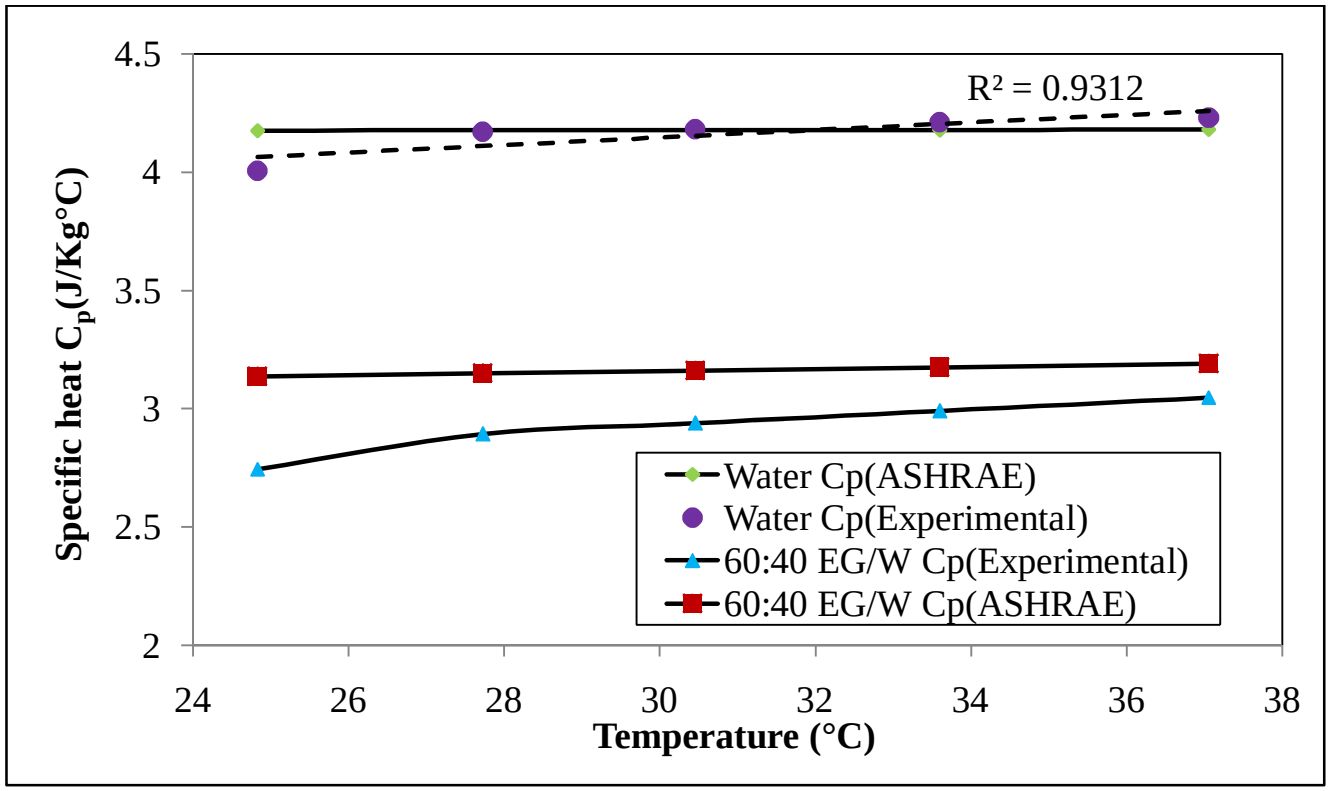

Figure 4.1: Comparison of specific heat of new experimental value of DI water (H_2O), Ethyl Glycol (EG) with ASHRAE (1994) DI water (H_2O), Ethyl Glycol (EG) temperature.

Figure 3.1 shows specific heat verses temperature graph deionized water and ethyl glycol. In order to obtain the trend of increase of specific heat, suitable trend line is drawn for each particle size with their corresponding equation and R^2 (R: correlation coefficient) values. It is concluded from the Figure 4.1 that there may be linear variation of specific heat with temperature. It is concluded from Figure 4.1 that with increase in temperature both experimental and Ashrae value increases and the experimental value of water was much closer to that of the data handbook ASHRAE (1994) value. It is also seen that the EG(60:40) experimental value is very close to that of the data handbook of ASHRAE (1994).

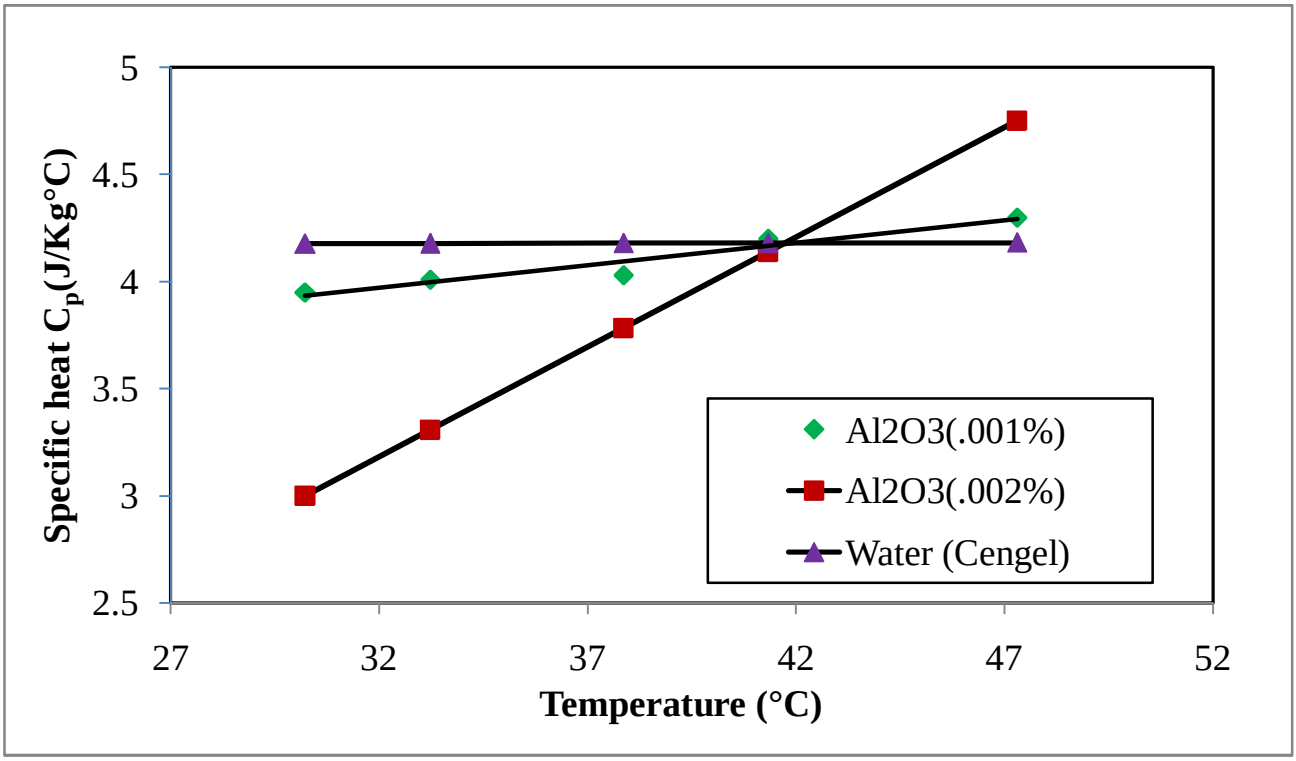

Figure 4.2: Comparison of specific heat of new experimental value of Al_2O_3(0.001%), Al_2O_3 (0.002%) 40nm with ASHRAE (1994) water (DI) .

Figure 4.2 shows consolidated data obtained from experiments of Al_2O_3-water based nanofluids. The variation of specific heat with temperature at .001% volume fraction of Al_2O_3 nanoparticles and at 40nm sizes of Al_2O_3 nanoparticles of diameter is shown in Figure 4.2. Al_2O_3 particles of 0.002% volume fraction in deionized water show higher enhancement in specific heat of Al_2O_3 particles than 0.001% volume fraction with linear trend. At 42^{o}C Al_2O_3 particles of alpha and gamma show same value of specific heat i.e. 4KJ/KgK.

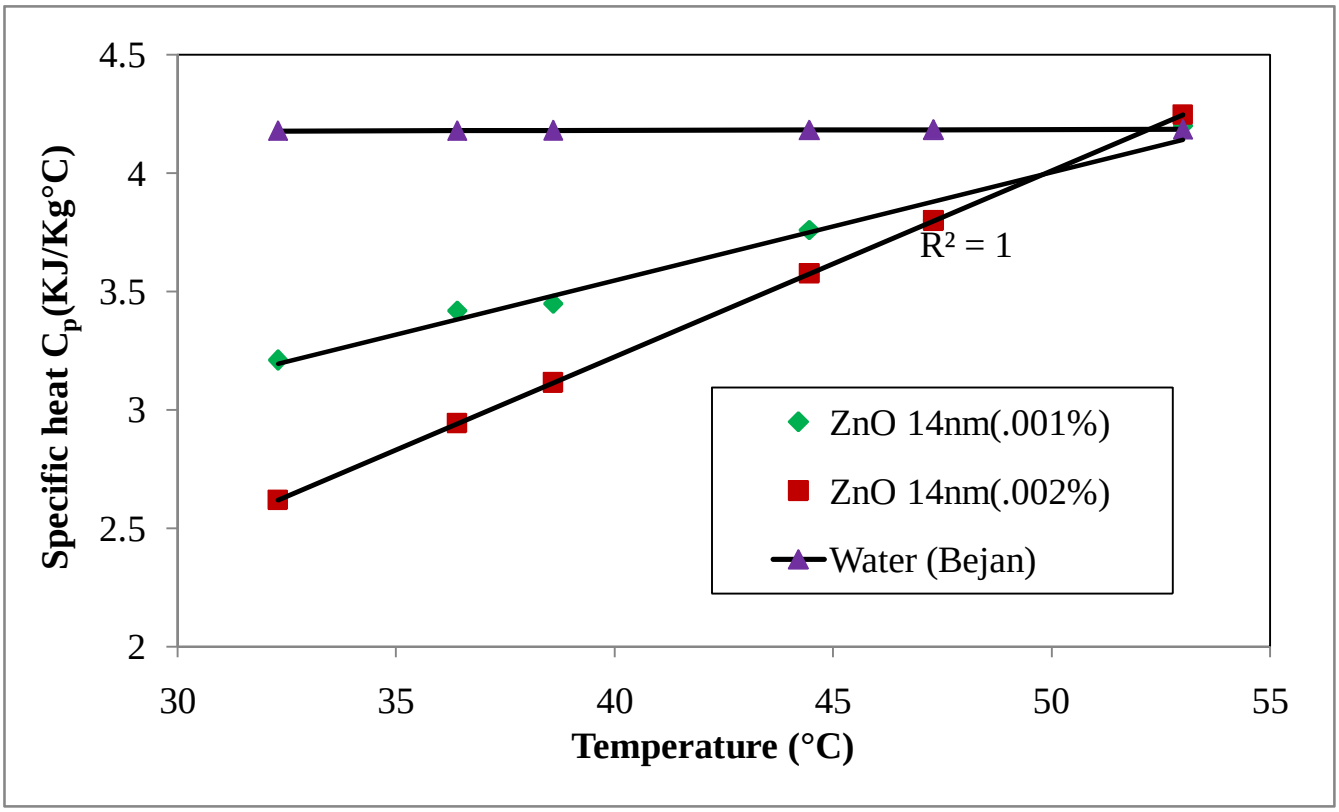

Figure 4.3: Comparison of specific heat of new experimental value of ZnO 14nm (0.001%), ZnO 14nm (0.002%) with Bejan Water(DI) at different temperature .

Figure 4.3 shows consolidated data from experiments of ZnO-water at 0.001% and 0.002% volume fraction and water (DI) from data handbook of Incropera et al, (1996). As shown in Figure 4.3 ZnO particles of 14 nm diameter of 0.001% volume fraction is more closer than to that of the ZnO of volume fraction 0.002% to that of the Incropera et al, (1996) data at different volume fraction with linear trend. As temperature increases, data points of both nanofluid (Al_2O_3-water (0.001%) and Al_2O_3-water (0.002%) are coming closer to each other (trend lines are converging) and at 50^{o}C data points of both the fluids (Al_2O_3-water (0.001%) and Al_2O_3-water (0.002%) are showing same value of specific heat i.e. 3.7.

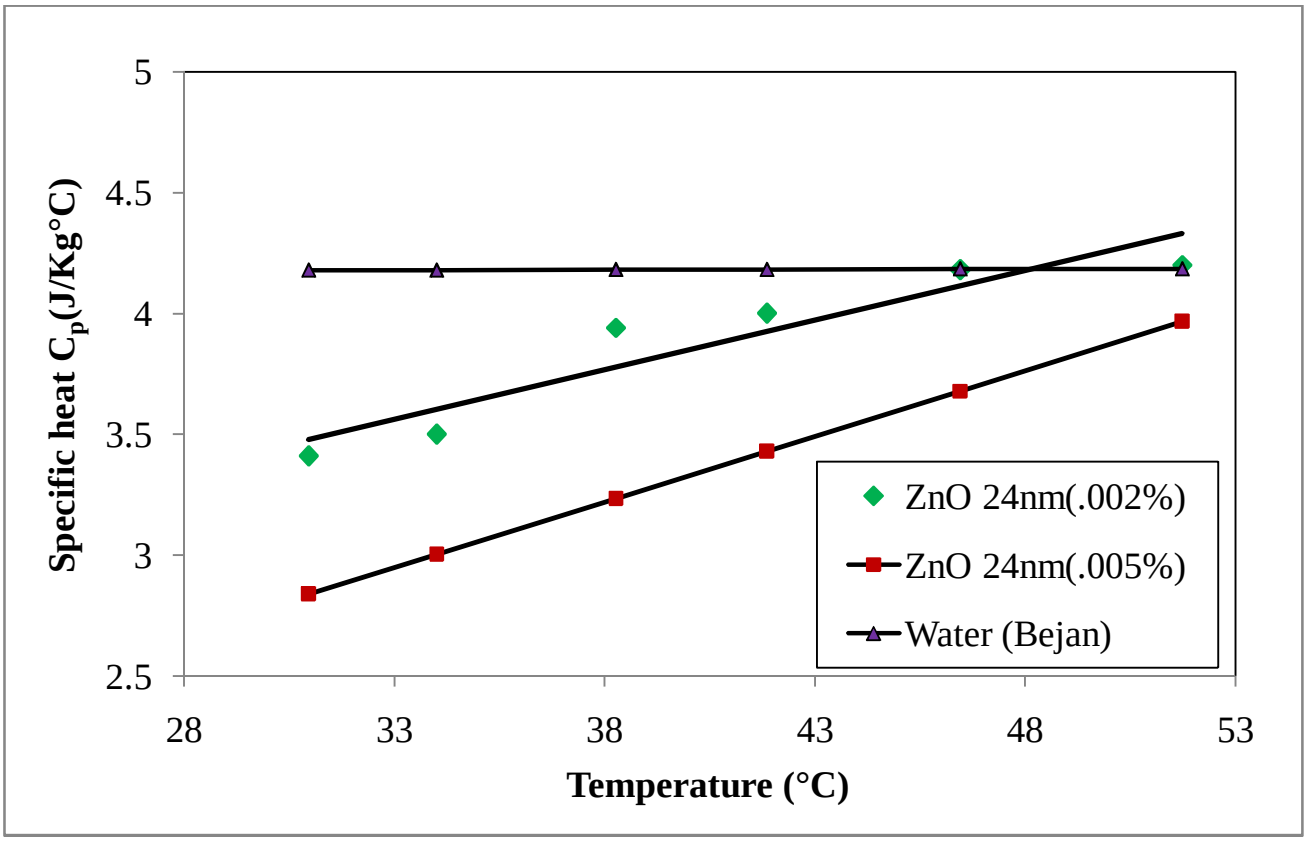

Figure 4.4: Comparison of specific heat of new experimental value of ZnO 24 nm (0.002%), ZnO 24nm (0.005%) with Bejan et al, (1996) Water (DI) at different temperature.

Figure 4.4 shows that at 0.002% volume fraction 24 nm diameter ZnO particles in water provides higher specific heat than 0.005% volume fraction with linear trend. So it is concluded that for any particle size specific heat increases with increase in temperature and ZnO 24nm (0.002%) nanofluid shows more enhancement in specific heat than for ZnO 24nm (0.005%) nanofluid for same particle size.

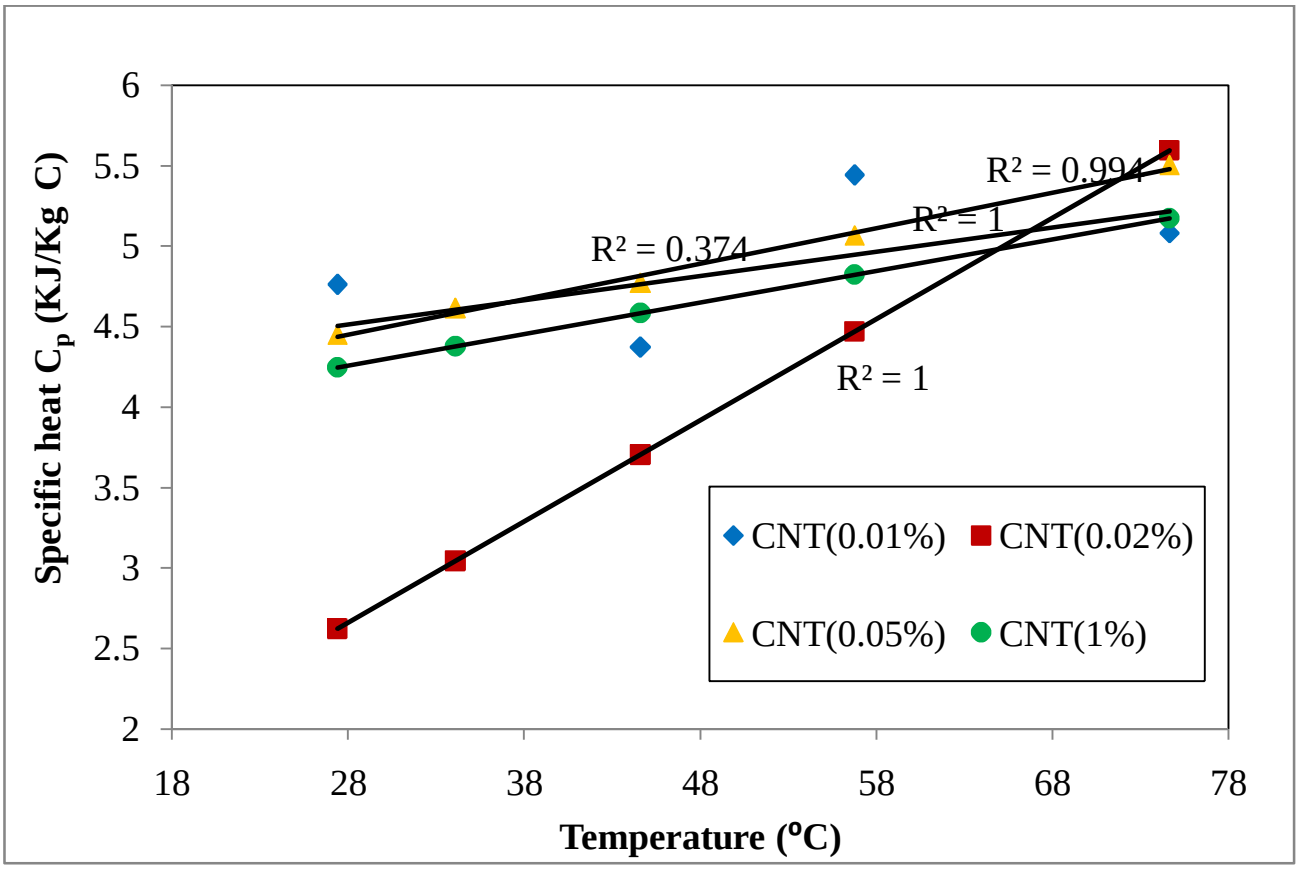

Figure 4.5: Comparison of specific heat of new experimental value of SWCNT 1nm (0.01%), SWNCT 1nm (0.02%), SWNCT 1nm (0.05%), SWNCT 1nm (1%) verses temperature.

Figure 4.5 is showing specific heat increases as size of SWNCT nanoparticles decreases with linear trend. At volume fraction of 0.01, 0.02, 0.05 and1 of SWNCT particles of 1 nm diameter are overlapping. At temperature of 68°C SWNCT particles of 1 nm diameter are overlapping and is having specific heat of 4.5. Nanoparticles of volume fraction 0.01, 0.05 and 1 showing marginal difference in specific heat. It is very clear from these nanofluids that with the increase in temperature specific heat increases if it is having different volume concentration of same material than also.

CHAPTER 5: DEVELOPMENT OF NEW MODEL FOR SPECIFIC HEAT OF NANOFLUIDS FROM NEW EXPERIMENTAL SET UP

In this chapter, new model have been developed to measure the specific heat of Al_2O_3-water, SWCNT, ZnO-water and silver nanofluids. Models have been developed by considering the fact that specific heat of nanofluid depends on so many parameters.

5.1 Development of Models for Specific Heat for Nanofluids

Specific heat of nanofluid depends on the various parameter like diameter , temperature, viscosity of the fluid, density of particle and base fluid, specific heat of particle and that of nanofluid and volume fraction. Specific heat of nanofluid is believed to be depending on various particle and fluid properties, as given by:

$$C_{pnf} = f(d, T, Ц\, \rho_f, \rho_P, C_{P_P}, C_{P_f}, \emptyset) \tag{5.1}$$

or

$$f_1(d, T, Ц\, \rho_f, \rho_P, C_{P_P}, C_{P_f}, \emptyset)$$

Using Buckingham Pi theorem, the following dimensionless groups have been obtained:

$$\pi_1 = \frac{d^2\, T\rho_P^2 C_{pf}}{\mu^2}, \qquad \pi_2 = \frac{\rho_f}{\rho_p}, \qquad \pi_3 = \frac{d^2 T\rho_p^2\, c_{P_p}}{\mu^2}, \qquad \pi_4 = \frac{d^2 T\rho_p^2 c_{p_f}}{\mu^2}, \qquad \pi_5 = \emptyset$$

Experimental data for Al_2O_3-water nanofluids ZnO-water nanofluids and SWCNT for a wide range of volume fraction, particle size and temperature, the following models has been derived using regression analysis. Model given in equation 5.2 is for Al_2O_3-water nanofluids, ZnO, SWCNT.

Finally the specific heat of nanofluid from the dimensionless analysis are as shown below :

$$C_{nf} = 0.152 \ \frac{\mu^2}{d^2 T \rho_P^2} \ \left(\frac{\rho_f}{\rho_p}\right)^{2.28} \left(\frac{d^2 T \rho_p^2 c_{P_p}}{\mu^2}\right)^{-1.62} \left(\frac{d^2 T \rho_p^2 c_{p_f}}{\mu^2}\right)^{2.81} \emptyset \qquad (5.2)$$

The temperature range for which the set up is design is upto 338K. The working condition of the system was low as it was difficult for insulation to prevent the heat to go out from the system.

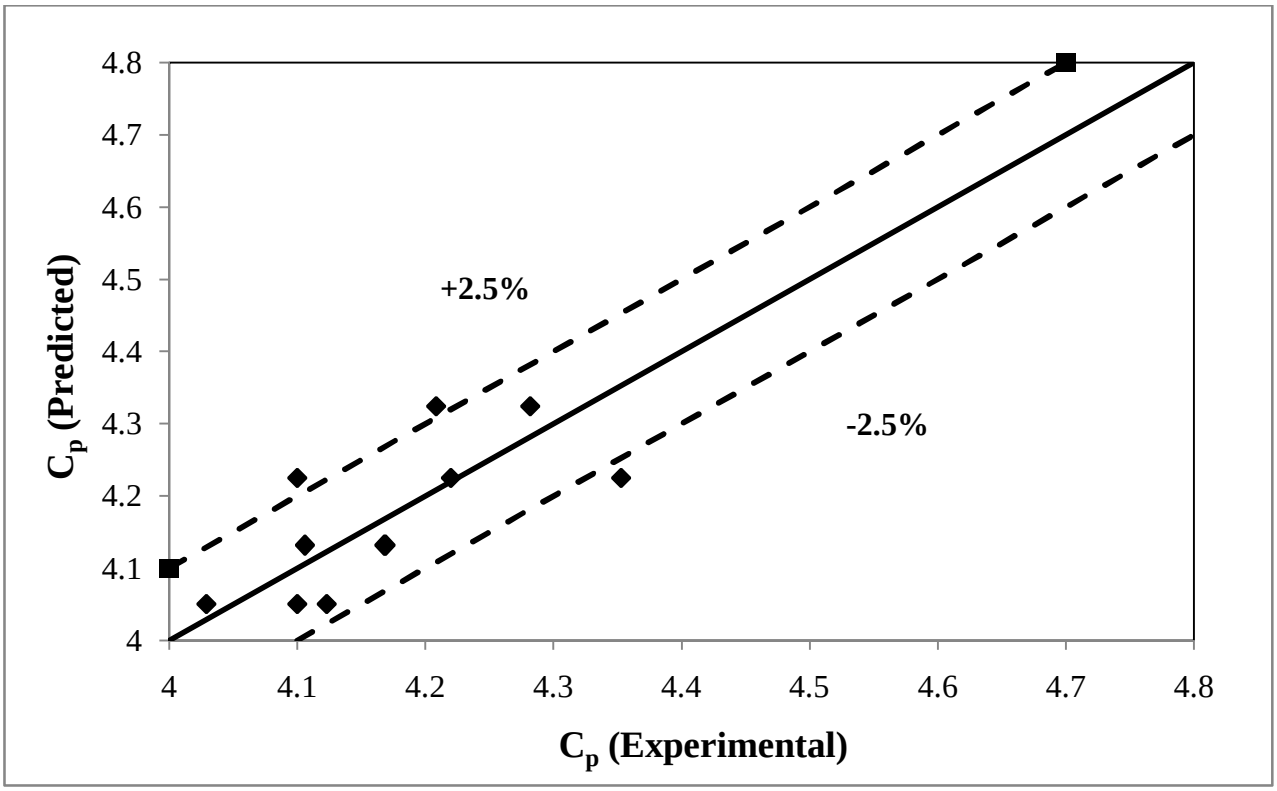

Figure 5.1: Experimental versus predicted values of specific heat for Al_2O_3-water(alpha) nanofluids using new model given (equation 5.2).

The above models have been used to predict the nanofluid specific heat and the predicted versus experimental values of specific heat of nanofluids are provided in Figure 5.1 (for of Al_2O_3-water nanifluids). The comparison plots show that the new model generally predicts within ±2.5% accuracy range for Al_2O_3(alpha)-water nanofluids.

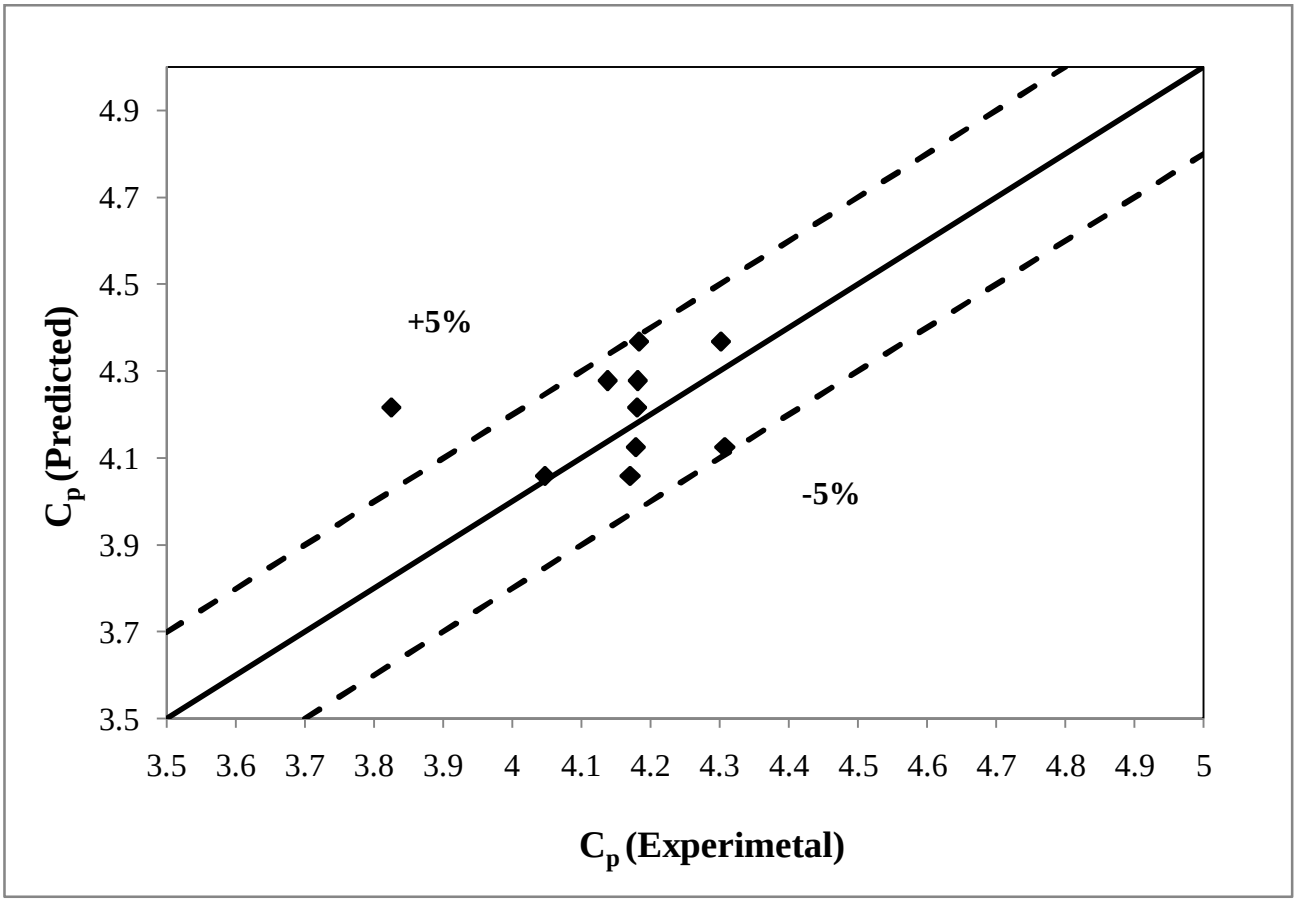

Figure 5.2: Experimental versus predicted values of specific heat for Al_2O_3-water(gamma) nanofluids using new model given (equation 5.2).

The comparison plots show that the new model generally predicts within ±5% accuracy range for Al_2O_3-water(gamma) nanofluids.

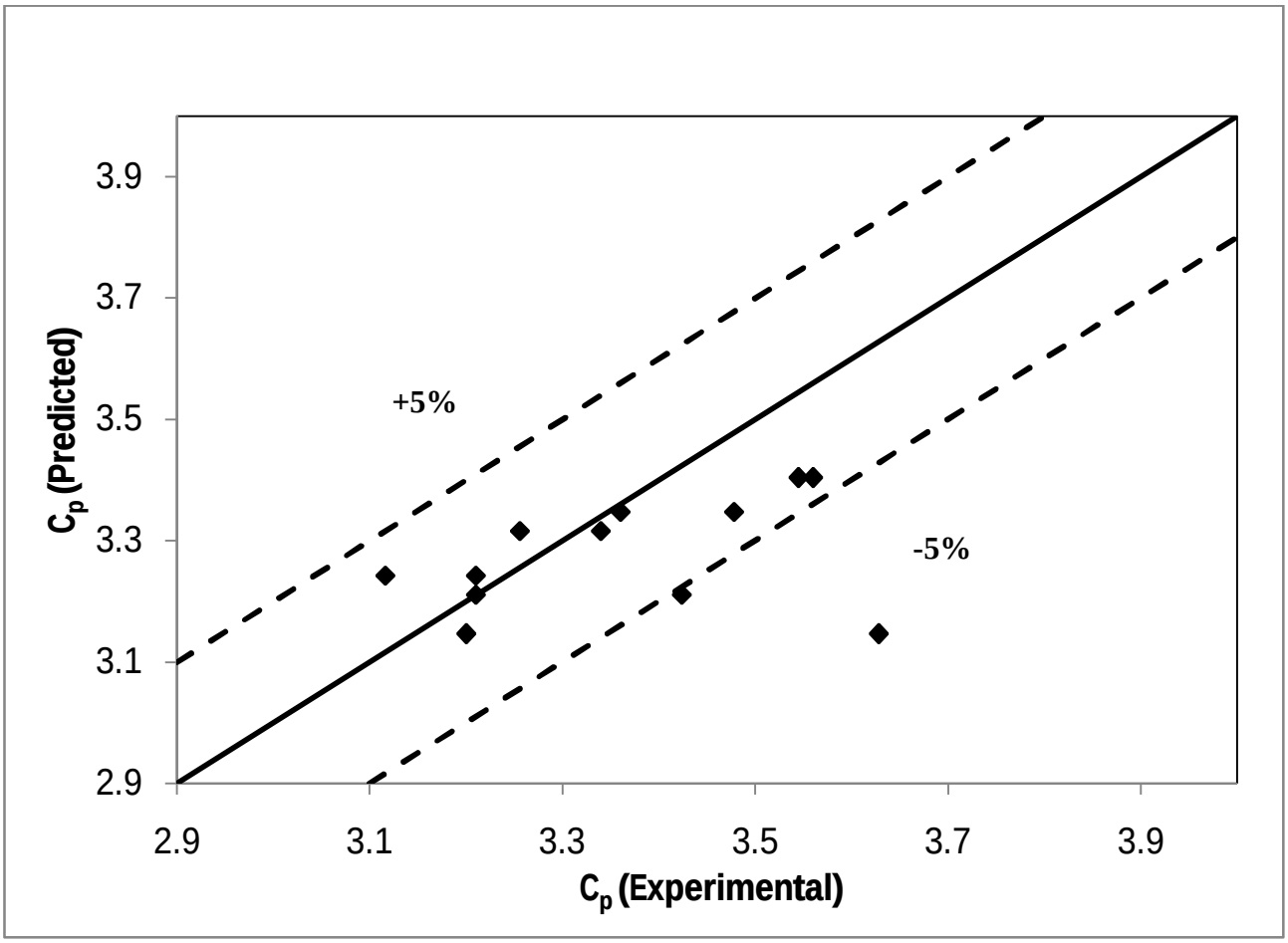

Figure 5.3: Experimental versus predicted values of specific heat for ZnO(14 nm) nanofluids using new model given (equation 5.2).

The comparison plots show that the new model generally predicts within $\pm 5\%$ accuracy range for ZnO (14 nm) nanofluids.

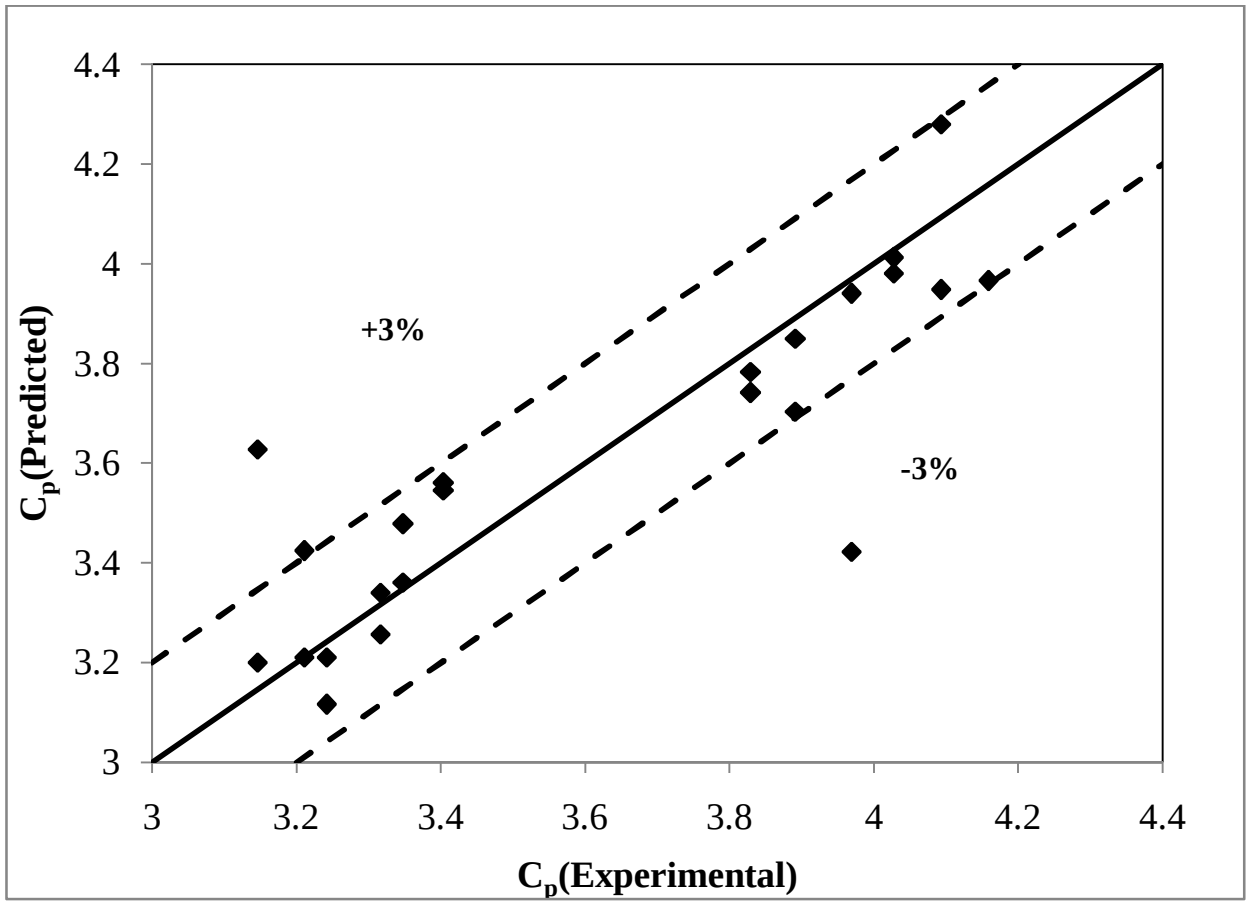

Figure 5.4: Experimental versus predicted values of specific heat for ZnO(24nm) nanofluids using new model given (equation 5.2).

The comparison plots show that the new model generally predicts within ±3% accuracy range for ZnO (14 nm) nanofluids.

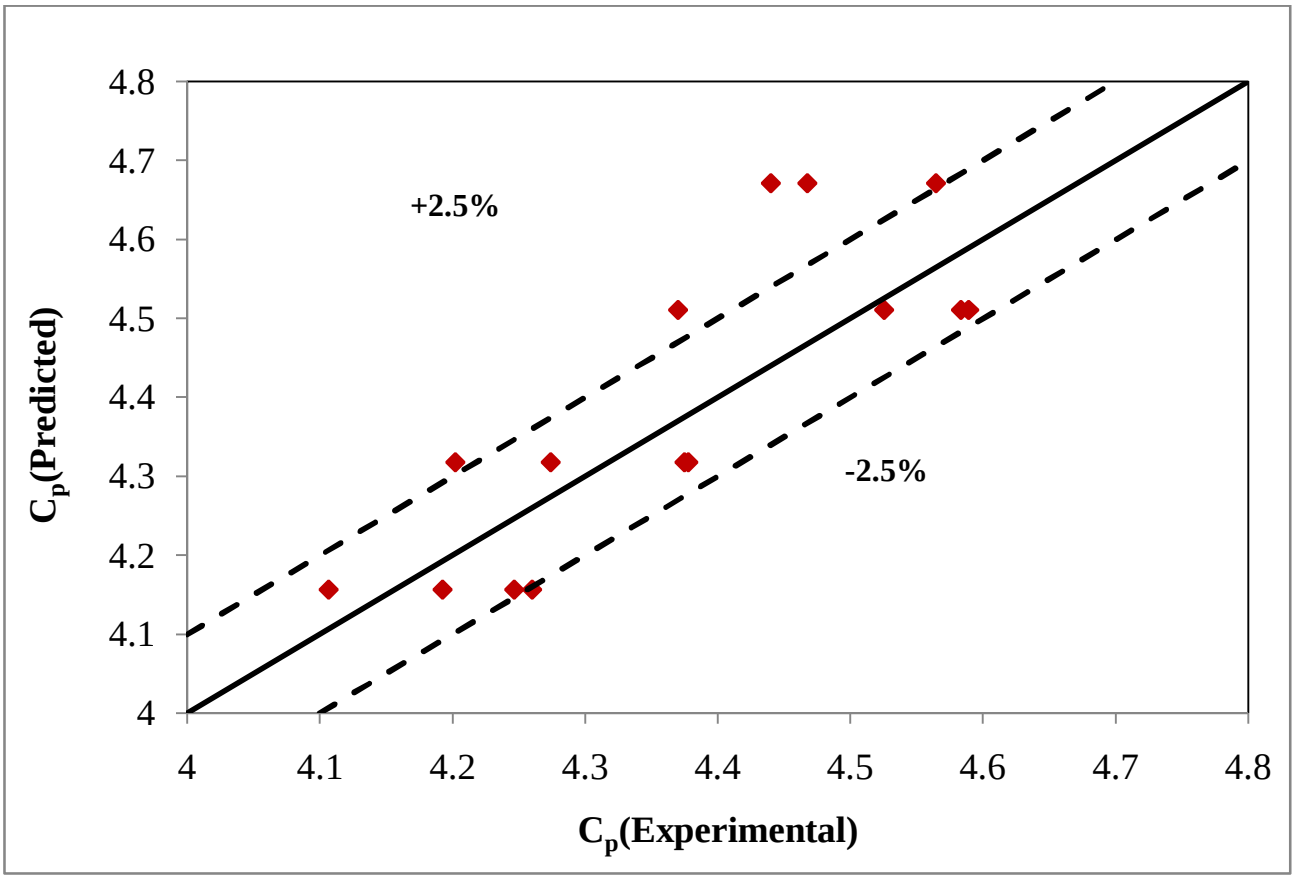

Figure 5.5: Experimental versus predicted values of specific heat for SWCNT (1nm) nanofluids using new model given (equation 5.2).

The comparison plots show that the new model generally predicts within ±2.5% accuracy range for SWCNT (1nm) nanofluids.

5.2 Validation of New Developed Models:

The above models (equation 5.2) has been further evaluated by using it to predict the nanofluid specific heat for a range of experimental conditions and by comparing the predicted versus experimental values.

In Figure 5.3, experimental values of specific heat obtained from Li and Peterson (2007) for Al_2O_3 nanoparticles of diameter 36 nm, 35.5^oC temperature and given volume fraction range are compared with that obtained from new developed model for Al_2O_3 (equation 5.2).

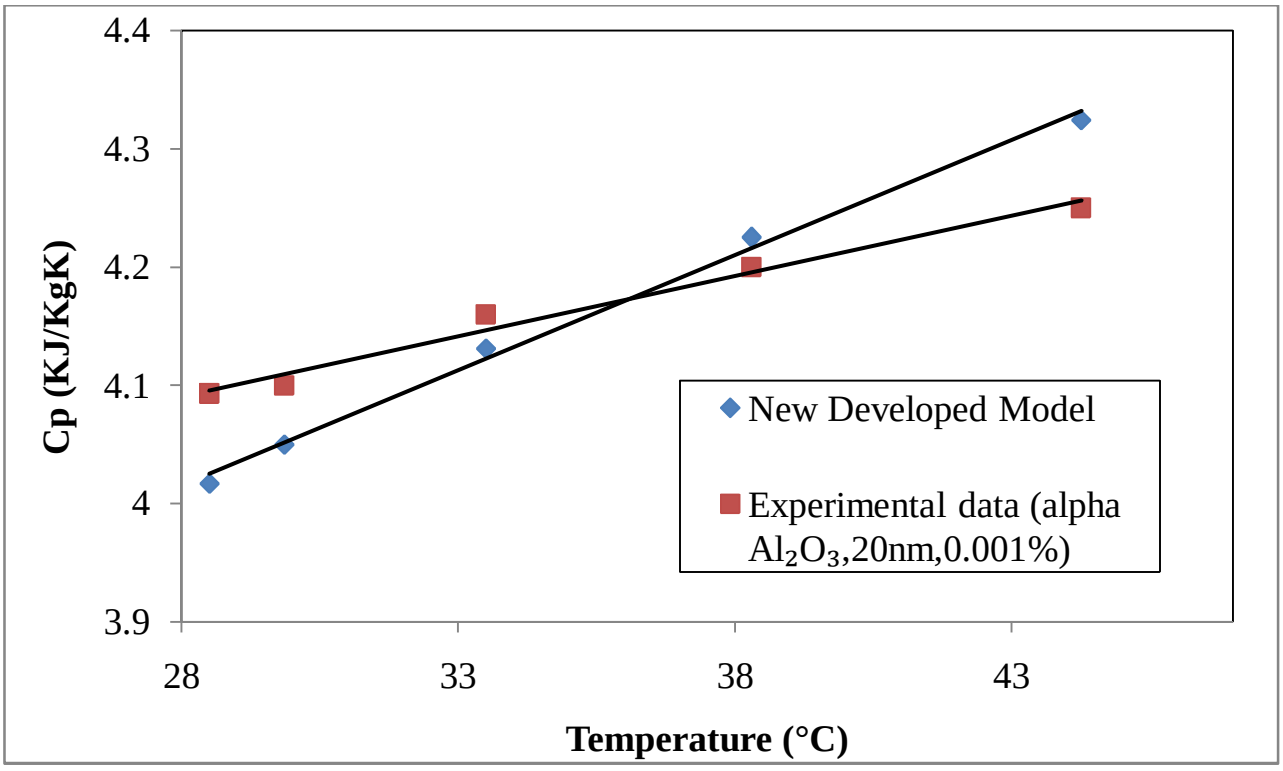

Figure 5.3: Experimental versus predicted values (present model) of specific heat with increase in temperature, d: 40 nm, ø=0.001%.

Figure 5.3 shows that the specific heat obtained from new developed model under predict the experimental value. It shows that below 40°C new developed model over predict the experimental values and above 40°C model under predict the experimental values. In Figure 5.4, experimental values of specific heat obtained for alpha Al_2O_3 nanoparticles of diameter 40 nm, 0.002% volume fraction and given temperature range are compared with that obtained from new developed model for alpha Al_2O_3 (equation 5.2).

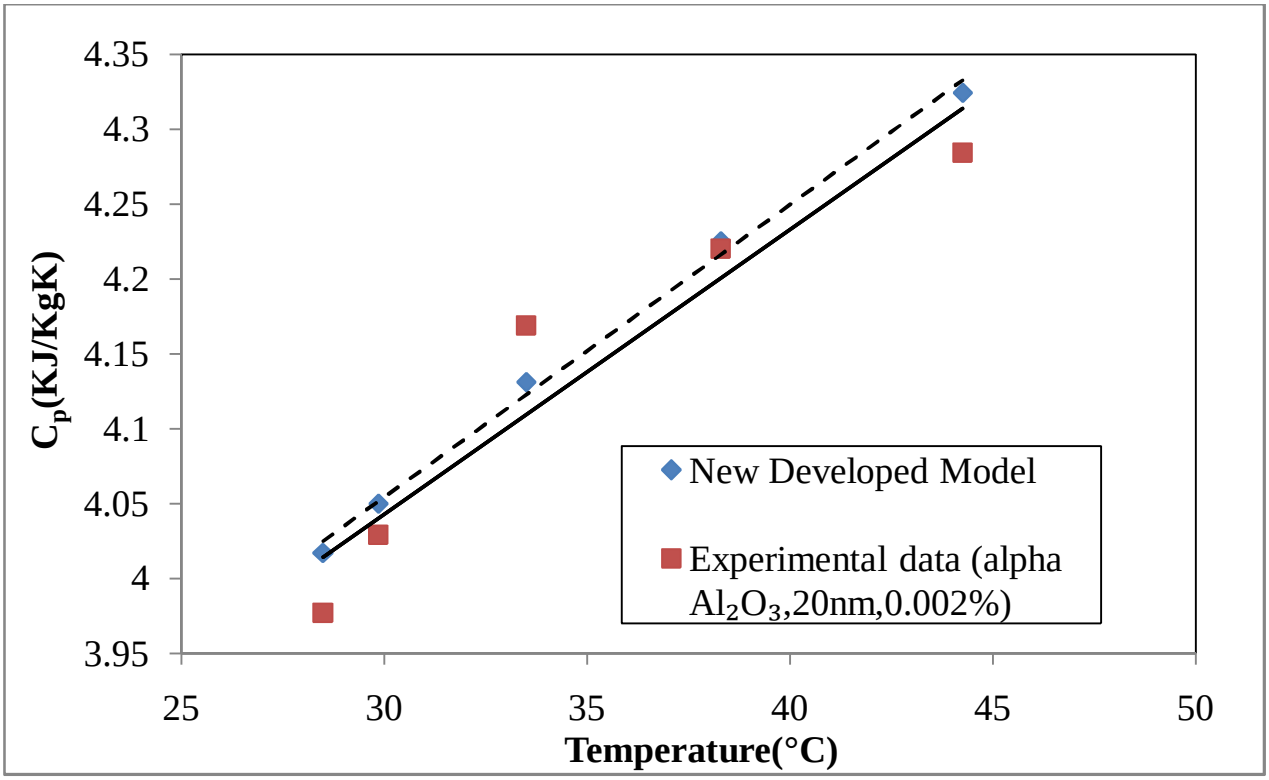

Figure 5.4: Experimental versus predicted values (present model) of specific heat with increase in temperature of alpha Al_2O_3 nanoparticles, d: 40 nm, φ: 0.002%.

Figure 5.4 The trend of predictions obtained using new developed model is almost parallel to the experimental data. Specific heat obtained from experiment and model increases with increase in temperature. In Figure 5.5, experimental values of specific heat obtained for alpha Al_2O_3

nanoparticles of diameter 40 nm, of volume fraction 0.005% range are compared with that obtained from the new developed model for Al_2O_3 (equation 5.2).

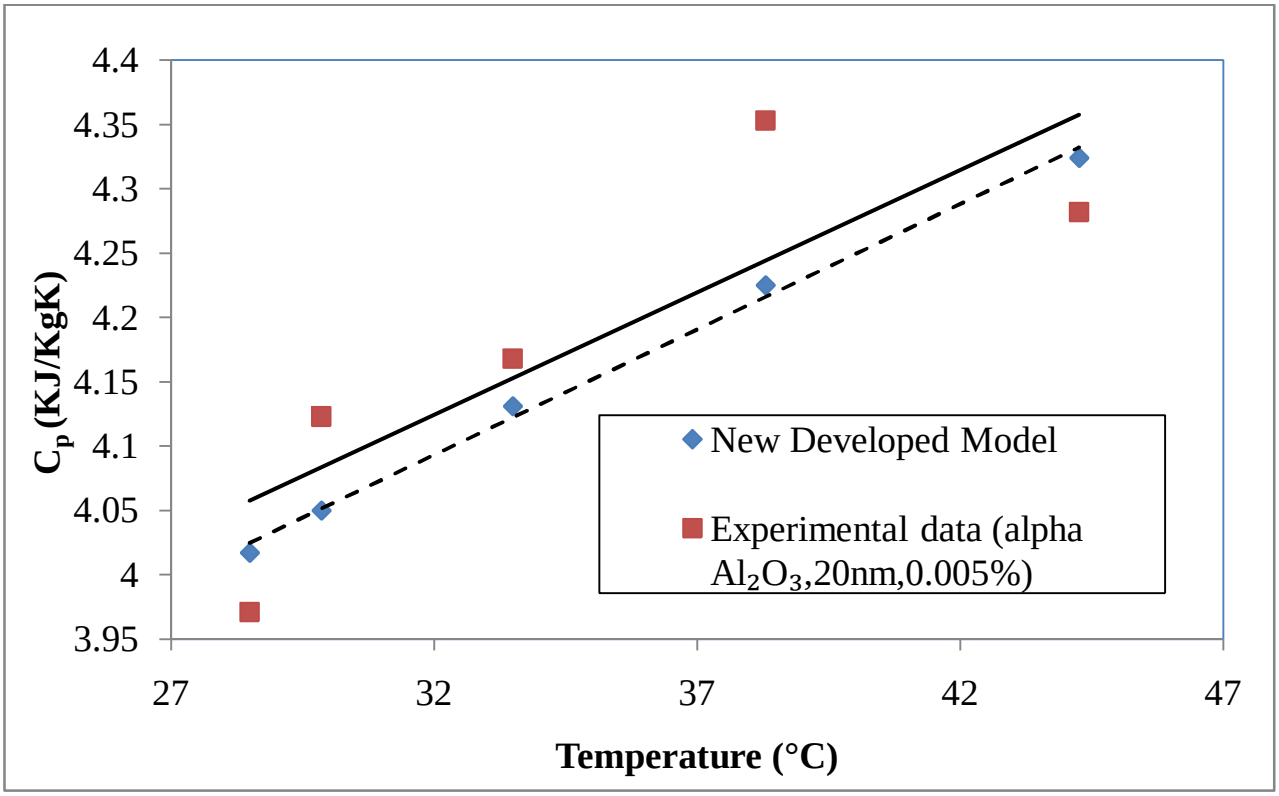

Figure 5.5: Experimental versus predicted values (present model) of specific heat with increase in temperature of alpha Al_2O_3 nanoparticles, d: 40 nm, ⍰: 0.005%.

Figure 5.5 shows that values of specific heat obtained from new developed model are very close to that obtained from experiment. Specific heat increases with increase in temperature. Experimental values of specific heat obtained for alpha Al_2O_3 nanoparticles of diameter 40 nm, volume fraction(ø): 0.005% are compared with that obtained from new developed model for Al_2O_3 (equation 5.2) .

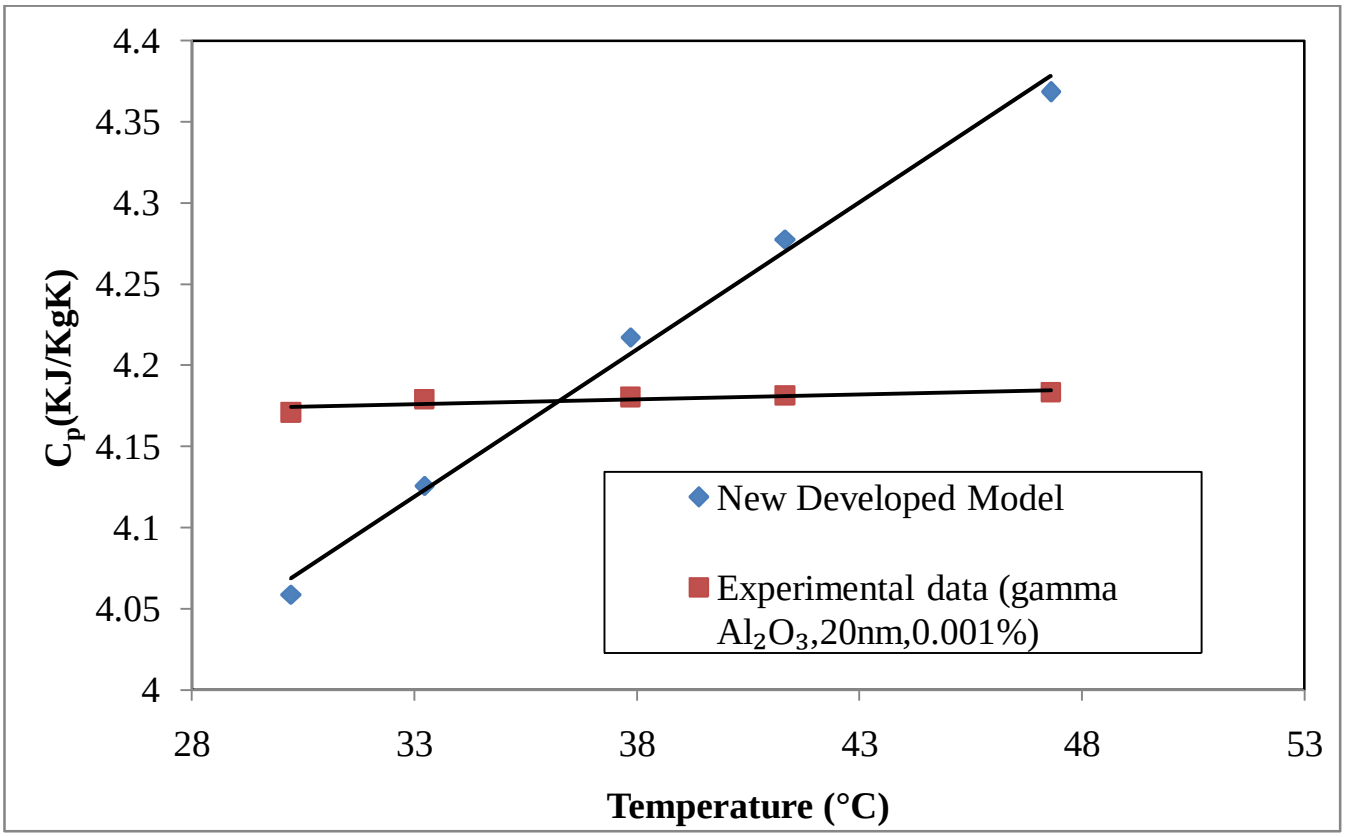

Figure 5.6: Experimental versus predicted values (present model) of specific heat with increase in temperature of gamma Al_2O_3 nanoparticles, d: 40 nm, □: 0.001%.

In Figure 5.6 specific heat obtained from model under predicts the experimental values. Specific heat increases with increase in temperature. Experimental values of temperature obtained for gamma Al_2O_3 nanoparticles of diameter 20 nm, and given volume fraction range are compared with that obtained from new developed model for gamma Al_2O_3 (equation 5.3) .

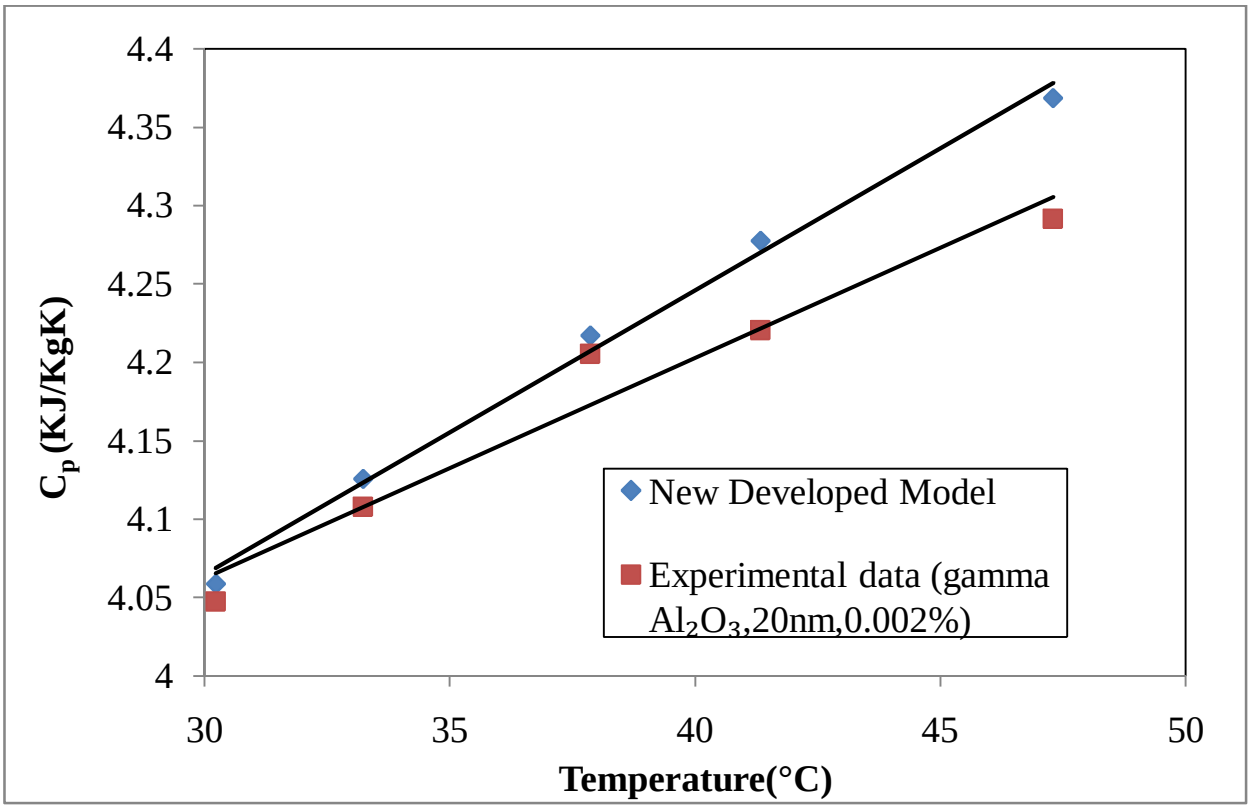

Figure 5.7: Experimental versus predicted values (present model) of specific heat with increase in temperature of gamma Al_2O_3 nanoparticles, d: 40 nm, □: 0.002%.

In Figure 5.7 specific heat obtained from model over predicts the experimental values. Specific heat increases with increase in temperature. Experimental values of specific heat obtained for gamma Al_2O_3 nanoparticles of diameter 20 nm, and given volume fraction are compared with that obtained from new developed model for gamma Al_2O_3 (equation 5.3) .

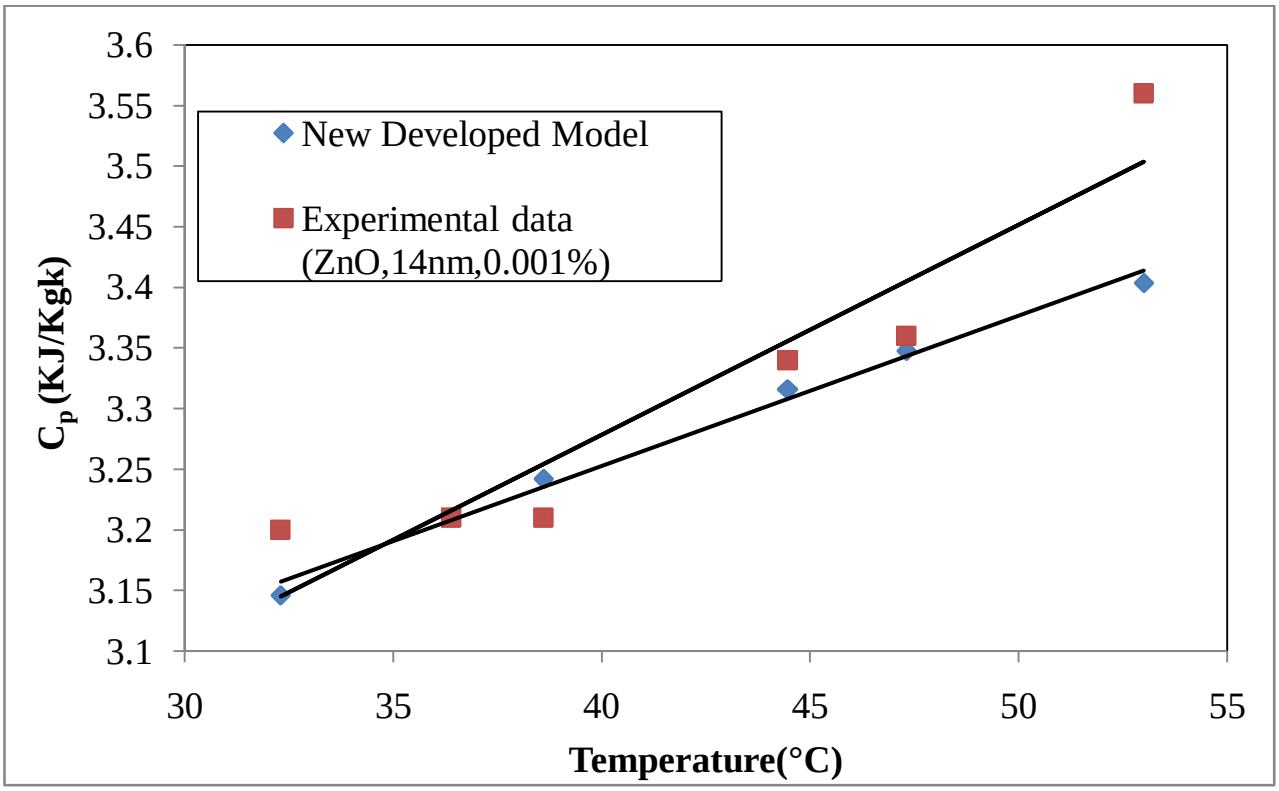

Figure 5.8: Experimental versus predicted values (present model) of specific heat with increase in temperature of ZnO, d: 14 nm, ⍰: 0.001%

In Figure 5.8, experimental values of specific heat obtained for ZnO nanoparticles of diameter 14 nm, and given volume fraction 0.001% range are compared with that obtained from new developed model for ZnO (equation 5.2). Figure 5.8 shows that the specific heat obtained from new developed model under predict the experimental value. In Figure 5.8, experimental values of specific heat obtained ZnO nanoparticles of diameter 14 nm, 0.001% volume fraction and given temperature range are compared with that obtained from new developed model for ZnO (equation 5.2).

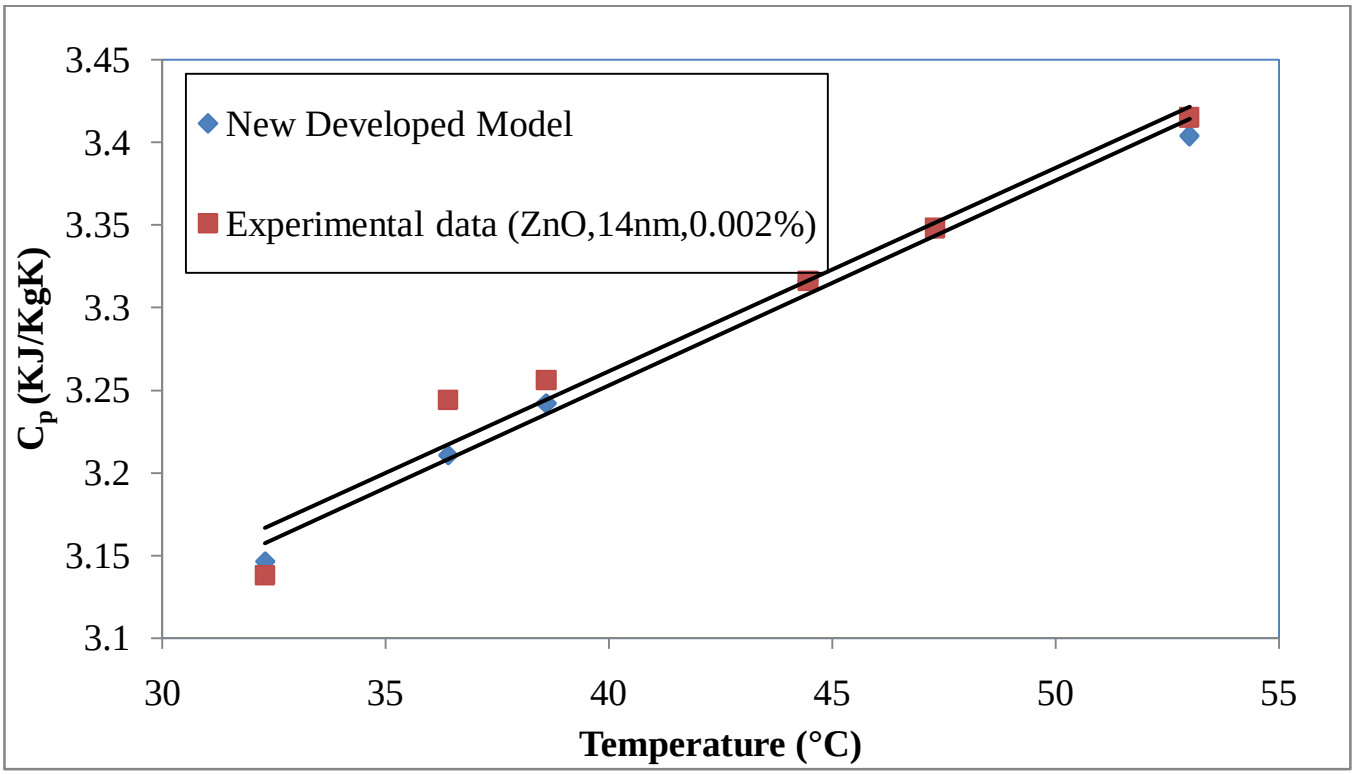

Figure 5.9: Experimental versus predicted values (present model) of specific heat with increase in temperature of ZnO, d: 14 nm, □: 0.002%

In Figure 5.9, experimental values of specific heat obtained ZnO nanoparticles of diameter 14 nm, given volume fraction 0.002% and temperature range are compared with that obtained from new developed model (equation 5.2).

Figure 5.9 shows that the specific heat obtained from new developed model under predict the experimental value. The trend of predictions obtained using new developed model is almost parallel to the experimental data.

In Figure 5.10, experimental values of specific heat obtained for ZnO nanoparticles of diameter 24 nm, 0.002% volume fraction and given temperature range are compared with that obtained from new developed model for ZnO (equation 5.2).

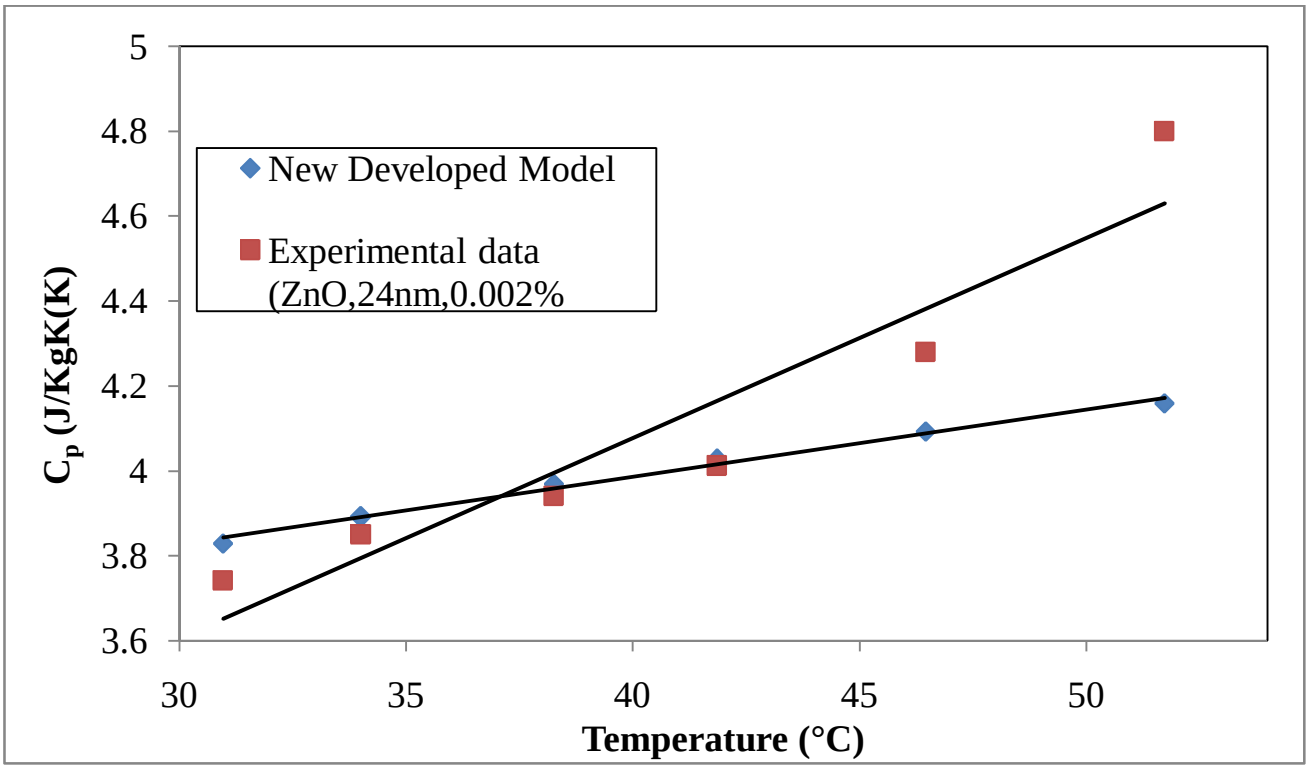

Figure 5.10: Experimental versus predicted values (present model) of specific heat with increase in temperature, d: 24 nm, ⍰: 0.002%

Figure 5.10 shows that below 40^{o}C new developed model over predict the experimental values and above 40^{o}C model under predict the experimental values. Specific heat obtained from experiment and model increases with increase in temperature. In Figure 5.10, experimental values of specific heat obtained for ZnO nanoparticles of diameter 24 nm, different temperature range and given volume fraction are compared with that obtained from the new developed model for ZnO (equation 5.2).

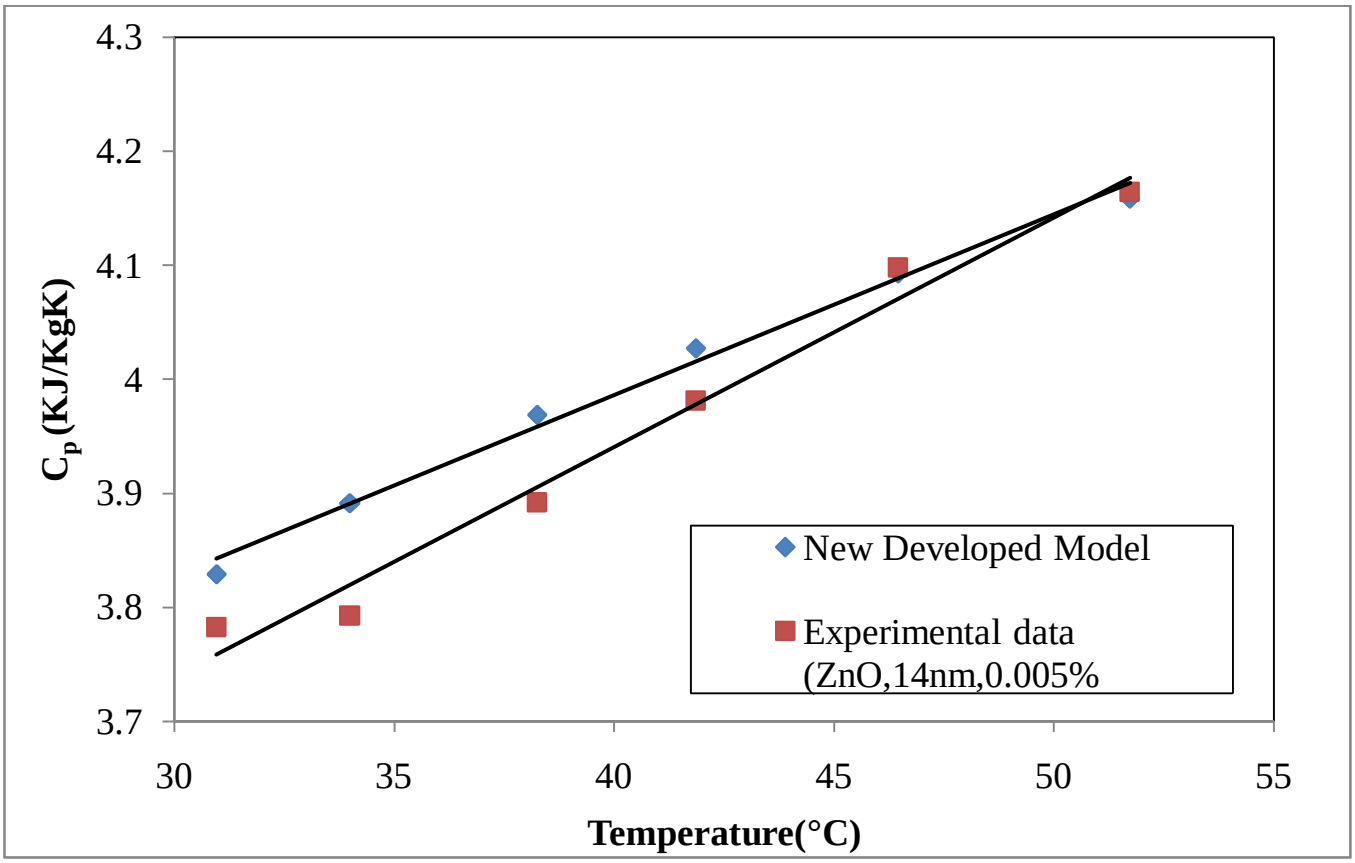

Figure 5.11: Experimental versus predicted values (present model) of specific heat with increase in temperature ZnO, d: 14 nm, □: 0.002%.

Figure 5.11 shows that values of specific heat obtained from new developed model are very close to that obtained from experiment. Specific heat increases with increase in temperature. Experimental values of specific heat obtained for ZnO nanoparticles of diameter 14 nm, 0.002% volume fraction and temperature range are compared with that obtained from new developed model for ZnO (equation 5.2) in Figure 5.11.

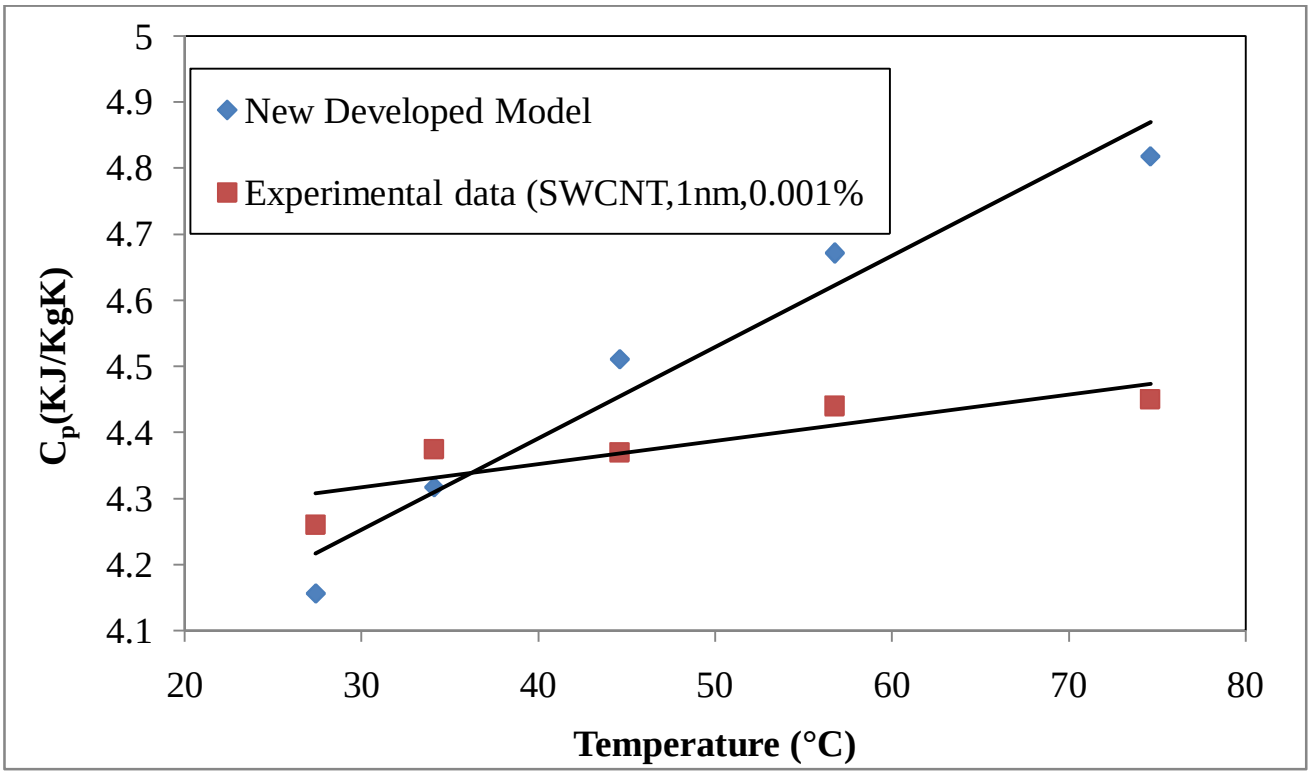

Figure 5.12: Experimental versus predicted values (present model) of specific heat with increase in temperature SWCNT, d: 1 nm, □: 0.001%.

Figure 5.12 shows that the specific heat obtained from new developed model under predict the experimental value. The trend of predictions obtained using new developed model is almost parallel to the experimental data. In Figure 5.12, experimental values of specific heat obtained for SWCNT nanoparticles of diameter 1 nm, 0.001% volume fraction and given temperature range are compared with that obtained from new developed model for SWCNT (equation 5.2).

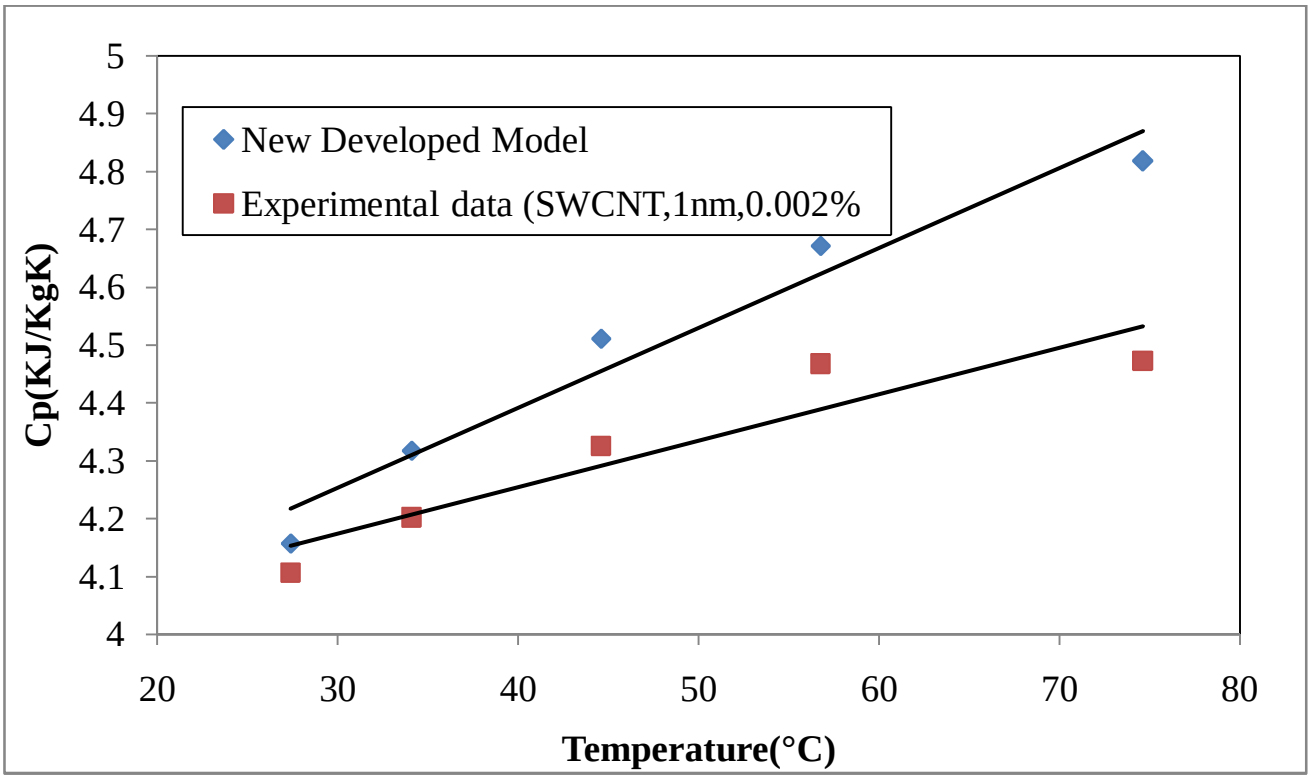

Figure 5.13: Experimental versus predicted values (present model) of specific heat with increase in temperature SWCNT, d: 1 nm, □: 0.002%.

Figure 5.13 shows that the specific heat obtained from new developed model under predict the experimental value. The trend of predictions obtained using new developed model is almost parallel to the experimental data.

In Figure 5.14, experimental values of specific heat obtained for SWCNT nanoparticles of diameter 1 nm, 0.005% volume fraction and given temperature range are compared with that obtained from new developed model for SWCNT (equation 5.2).

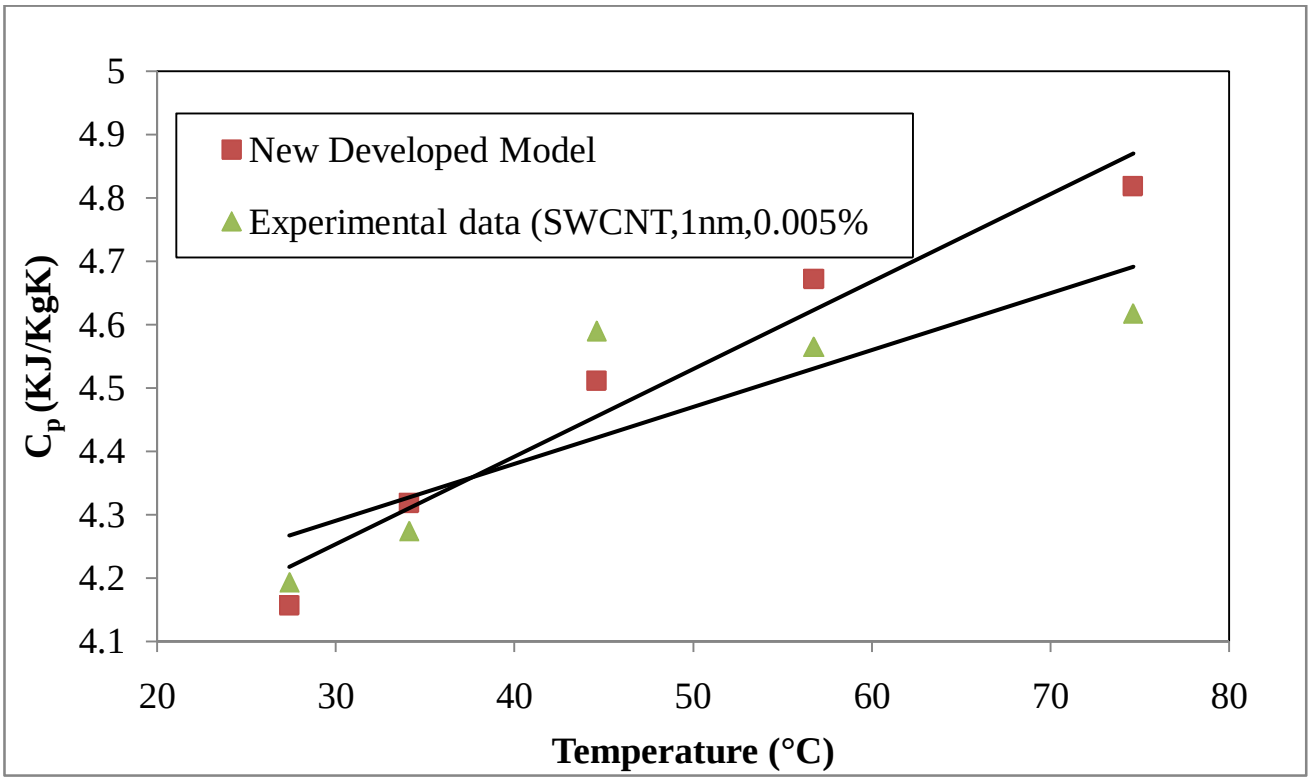

Figure 5.14: Experimental versus predicted values (present model) of specific heat with increase in temperature SWCNT, d: 1 nm, □: 0.002%.

Figure 5.14 shows that values of specific heat obtained from new developed model are very close to that obtained from experiment. Specific heat increases with increase in temperature. Experimental values of specific heat obtained for SWCNT nanoparticles of diameter 1 nm, 0.002% volume fraction and different temperature range are compared with that obtained from new developed model for SWCNT (equation 5.2) in Figure 5.14.

CHAPTER 6: CONCLUSION AND FUTURE SCOPE OF WORK

6.1 Conclusion

1. Specific heat of nanofluids increases with increase in temperature of nanoparticles in base fluid, volume fraction of nanofluids and also increases with size of nanoparticles.

2. A new specific heat model has been developed using dimensionless analysis. The new models have been found to generally predict specific heat of nanofluids within $\pm 2.5\%$ accuracy range for Al_2O_3-water naofluids and $\pm 5\%$ accuracy range for ZnO-water nanofluids and $\pm 5\%$ accuracy range for SWCNT.

3. The new developed set up for specific heat worked fantastically at temperature range of 298K to 308K. This temperature range best suited for this setup for measuring both water and nanofluid.

4. The new developed model gave good result when compared with different nanofluid of SWCNT, Al_2O_3, ZnO, Ethyl Glycol.

6.2 Future Scope of Work

1. More fundamental study has to be carried out on the effect of different parameters on specific heat of nanofluids.

2. A standard theoretical model for nanofluid specific heat has to be developed by taking consideration of all the possible mechanisms such as interfacial layer, phonon vibration, clustering etc and effect of other factor such as shape, ultrasonication time and pH.

3. A standard design of experiment for specific heat of nanofluid can be proposed by doing efficient number of experiments over wide range of variables.

4. Further studies are required to better understand the mechanism of specific heat through nanofluids and the influence of different experimental conditions on the specific heat of nanofluids for more accurate modelling.

APPENDIX

Appendix A

TABLE A.1: Specific heat of **TNT (0.01%)**

T (min)	V	I	T1	T2	T3	T4	T5	T6	T7	T8	T9	T10	T11	Variac	Specific Heat(Cp)
5	0	24.2	23.1	25.2	24.3	25	23	23.1	23.3	23.2	23.2	23.6	24	0	
5	28	1.06	24.6	23.5	31.2	27.3	29.3	25.8	23.2	23.3	23.3	23.3	24	30	3.11
5	38	1.41	26.2	25.2	39.3	33.5	36.8	32.1	23.1	23.5	23.3	23.5	25	40	3.21
5	48	1.81	32.4	31.2	52.1	44	48.3	41.7	23.5	23.6	23.5	24	25.5	50	3.53
5	57	2.14	38.3	37.5	65.6	55.8	60.9	53.6	24.4	24.3	24	25.9	26	60	3.62

TABLE A.2: Specific heat of **TNT (0.02%)**

T (min)	V	I	T1	T2	T3	T4	T5	T6	T7	T8	T9	T10	T11	Variac	Specific Heat(Cp)
5	0	-0.01	24	23.1	25.4	24.9	25.5	23.4	23.2	23.2	23.3	23.5	23	0	
5	28	1.10	25	24	31.8	28.9	30.3	26.6	23.3	23.3	23.3	23.7	23.1	28	4.3
5	38	1.40	27.6	26.6	43.6	36.8	40.8	35.2	23.6	23.5	23.5	24.6	24	38	4.37
5	48	1.87	34.8	33.3	53.8	46.1	50.8	43.9	23.8	23.8	23.8	25.2	25.5	48	4.35
5	57	2.21	40.3	39.2	70.9	59.9	66	58.1	24.7	24.6	24.2	28.4	26	57	4.37
5	68	2.61	55.8	53.2	85.1	76	82.1	73.6	25.5	25.2	24.8	39.9	30	68	4.4

TABLE A.3: Specific heat of **TNT (0.05%)**

T (min)	V	I	T1	T2	T3	T4	T5	T6	T7	T8	T9	T10	T11	Variac	Specific Heat(Cp)
5	0	-0.01	23.8	22.5	24.8	24.1	24.8	22.6	22.8	23	23	23.4	23	0	
5	29	1.06	24.2	22.9	29.3	26.4	28.4	24.8	22.9	23.2	23.1	23.5	23.5	29	4.21
5	37	1.38	25.6	24.2	38.6	32.8	36.9	31.4	23.1	23.3	23.2	23.8	23.5	37	4.22
5	48	1.81	30.9	29.2	50.9	42.3	48.2	40.6	23.3	23.4	23.3	24.3	24	48	4.23
5	60	2.24	36.2	34.2	67.3	55.5	63.3	54.2	24.1	24	23.6	26.9	25	60	4.25
5	69	2.61	50.1	46.6	84.3	73.2	80.9	70.9	24.4	24.3	24.1	32.3	26	69	4.3

TABLE A.4: Specific heat of **TNT (1%)**

T (min)	V	I	T1	T2	T3	T4	T5	T6	T7	T8	T9	T10	T11	Variac	Specific Heat(Cp)
5	0	-0.01	24.8	23.6	25.8	25.1	25.8	23.6	22.9	22.9	22.9	23.2	23	0	
5	27	1.05	25.6	24.5	31.2	28.4	30.3	26.8	23	23	23	23.2	23	27	4.33
5	37	1.43	26.8	25.9	39.5	33.9	37.2	32.5	23.5	23.2	23.2	23.5	23.5	37	4.42
5	40	1.88	32.6	31.6	52.6	44.4	48.8	42.5	23.4	23.3	23.3	24	24.9	40	4.61
5	59	2.27	38.1	37.8	70.3	59.2	65	57.4	24.2	24.1	23.8	26.3	26	59	4.65
5	68	2.62	53.4	52.5	85.3	75.8	81.3	73.5	25	24.8	24.2	32.2	33	68	4.67

TABLE A.5: Specific heat of **Ethyl Glycol (25%)**

T (min)	V	I	T1	T2	T3	T4	T5	T6	T7	T8	T9	T10	T11	Variac	Specific Heat(Cp)
5	1	-0.01	22.3	20.9	23.3	22.2	23.1	21.1	23.3	23.4	23.6	23.9	24	1	
5	26	0.98	22.6	21.6	28.4	25.3	26.9	23.5	23.5	23.6	23.8	23.9	23.8	26	4.31
5	36	1.36	24.4	23.3	35.3	30.9	33.6	29.4	23.6	23.6	24	24.3	24	36	4.38
5	50	1.88	29.1	27.9	49	40.9	44.9	38.6	23.8	23.9	24.1	24.9	25	50	4.41
5	60	2.26	34.8	34.1	65.5	56.1	61.9	54.2	24.4	24.3	24.9	24.9	25.1	60	4.52
5	70	2.65	51.5	49.8	83.8	74	79.4	71.1	25.3	25.3	25.2	39.9	30	70	4.61

TABLE A.6: Specific heat of **DI Water (500ml)**

Time(min)	Voltage (V)	Current (I)	T1	T2	T3	T4	T5	T6	T7	T8	T9	T10	T11	Variac	Specific Heat(Cp)
5	0	0	22.9	21.9	23.9	23	23.8	21.5	23.4	23.8	23.6	24.3	25	0	
5	21	0.79	23.2	22.3	26.5	24.8	25.8	23.9	23.6	23.8	24	24.4	25	21	4.03
5	27	1	27.8	27.3	35.8	33.5	34.7	32.6	24.2	24.3	24.3	24.9	25.2	27	4.02
5	35	1.32	34.9	34.2	43.1	40.6	41.6	41.9	39.8	26	26.3	25.5	26.8	35	4.03
5	40	1.52	36.8	36.4	49.8	46.9	48.4	46.4	26.3	26.8	27.3	27	27.7	40	4.14
5	45	1.70	42.4	42.3	58.5	55	56.4	54.4	26.5	26.6	26.1	27.6	27.5	45	4.17

TABLE A.7: Specific heat of **Ethyl Glycol (30%)**

T (min)	V	I	T1	T2	T3	T4	T5	T6	T7	T8	T9	T10	T11	Variac	Specific Heat(Cp)
5	0	0	24.3	23.3	25.2	24.2	25.1	22.9	25.3	25.3	25.6	25.9	27	0	
5	24	0.92	24.5	23.4	28.4	26.9	27.9	25.7	25.4	25.4	25.8	26.1	27.1	24	4.15
5	25	0.95	26	25.2	30.9	29.4	30.4	28.4	25.5	25.4	25.9	26.2	27.2	25	4.21
5	35	1.35	33.5	36.2	50.3	47.5	49	46.9	27.1	26.6	26.8	28.5	28.9	35	4.32
5	40	1.52	36.3	36.2	50.2	47.5	49	46.9	27.1	26.6	26.8	28.5	28.9	40	4.41
5	46	1.76	43.4	43.4	60.1	56.2	58.2	55.9	27.3	27	27.1	29.5	30	46	4.51

TABLE A.8: Specific heat of **Ethyl Glycol (50%)**

T (min)	V	I	T1	T2	T3	T4	T5	T6	T7	T8	T9	T10	T11	Variac	Specific Heat(Cp)
5	0	0	25	23.3	25.4	24.4	25.2	23.3	26.4	26.4	26.4	26	27.5	0	
5	22	0.84	25.1	23.5	28.4	26.9	27.7	26.3	26.4	26.4	26.4	26.6	27.5	22	3.12
5	24	0.90	25.8	24	29.9	29	29.9	27.6	26.8	26.5	26.6	26.9	27.5	24	3.23
5	29	1.09	31.8	29.9	40.6	38.8	39.8	36.9	28.1	27.9	27.3	27.8	28.5	29	3.33
5	32	1.23	32.9	30.9	42.9	41.1	42.3	42	30.1	28.5	27.6	28.3	29	32	3.24
5	37	1.41	36.3	34	48.9	47	48	45	29.4	28.9	27.9	28.9	29	37	3.67

TABLE A.9: Specific heat of **Silver (0.05%)**

T (min)	V	I	T1	T2	T3	T4	T5	T6	T7	T8	T9	T10	T11	Variac	Specific Heat(Cp)
5	0	-0.011	25	23.6	25.6	24.8	25.4	23.3	26.2	26.3	26.4	26.7	28	0	
5	21	0.78	25.1	24	27.8	26.2	26.9	26.1	26.3	26.4	26.4	26.8	28	21	3.75
5	24	0.90	25.5	24.4	29.9	28.5	29.1	28.8	26.3	26.3	26.6	26.9	28	24	4.1
5	26	0.98	26.9	26.3	33.6	31.4	32.3	31.5	26.4	26.4	26.7	26.9	28	26	4.5
5	28	1.05	28.3	27.6	36.8	34.8	35.9	35.1	26.9	26.6	26.8	27.3	28.1	28	4.6

TABLE A.10: Specific heat of **Alpha-aluminium oxide (0.0014%)**

T (min)	V	I	T1	T2	T3	T4	T5	T6	T7	T8	T9	T10	T11	Variac	Specific Heat(Cp)
5	0	-0.01	25.2	24.2	26.3	25.3	26.1	24.1	26.1	26.1	26.2	26.8	27.5	0	
5	22	0.80	25.3	24.3	30.1	28.6	28.9	28.1	26.3	26.2	26.3	26.9	27.6	22	3.93
5	24	0.90	25.4	25.3	32.4	30	30.8	28.8	26.2	26.2	26.4	26.8	27.9	24	4.3
5	28	1.06	26.8	25.9	35.6	33.3	33.9	37.3	26.5	26.4	26.7	27.5	28.5	28	4.4
5	30	1.12	28.3	28.2	42.8	38.3	39.3	37.3	26.5	26.7	26.5	27.7	28.5	30	4.7
5	33	1.26	30.4	30	48.5	43.5	45.3	44	27.1	26.8	26.9	28	29	33	5.1

TABLE A.11: Specific heat of **Alpha-aluminium oxide (0.002%)**

T (min)	V	I	T1	T2	T3	T4	T5	T6	T7	T8	T9	T10	T11	Variac	Specific Heat(Cp)
5	0	-0.01	26.2	25.2	28.2	27.2	28.2	25.9	25.2	25.4	26.1	27.2	28	0	
5	22	0.83	26.4	25.5	31.8	30.2	31.4	30.5	25.6	25.9	26.5	27.3	28	22	4.35
5	24	0.91	27.8	27.2	38.2	34.2	35.8	33.9	25.8	26.2	26.2	27.4	28	24	3.66
5	26	0.98	28.4	27.9	40.9	37	38.9	37.2	26.1	26.3	26.8	27.4	28	26	4.53
5	30	1.13	33.4	33.1	50.9	47.1	49	46.9	26.6	26.9	27.1	28.3	30	30	4.62
5	33	1.25	37.1	37.2	56.2	51.2	53.5	50.1	26.7	27.1	27.2	28.6	30.5	33	4.71

TABLE A.12: Specific heat of **Alpha-aluminium oxide (0.005%)**

T (min)	V	I	T1	T2	T3	T4	T5	T6	T7	T8	T9	T10	T11	Variac	Specific Heat(Cp)
5	0	0	24.1	23.3	26.8	25.8	26.8	24.5	22.8	23.1	23.6	26.2	29	0	
5	22	0.82	25.3	24.4	33.9	30.8	31.9	29.8	23.5	23.9	24.2	26.4	28	22	3.14
5	24	0.90	26.2	25.2	36.9	33.4	35.2	33.1	34.9	24	24.5	26.6	28	24	3.44
5	26	0.98	29	28.1	41.5	38.3	39	36.9	24.3	24.5	25.1	27.1	28.5	26	3.59
5	30	1.12	34.4	33.8	52.6	47.4	49.3	46.1	25.2	25.3	25.7	28.2	30	30	3.61
5	33	1.26	38.1	37.1	59.1	54.1	55.9	54	26.3	26.1	26.4	29.4	31	33	3.79

TABLE A.13: Specific heat of **Gamma-Aluminium Oxide (0.001%)**

T (min)	V	I	T1	T2	T3	T4	T5	T6	T7	T8	T9	T10	T11	Variac	Specific Heat(Cp)
5	0	-0.01	26.8	25.6	28.1	27	27.9	25.6	26.7	26.7	27.2	27.6	28	0	
5	22	0.83	26.8	25.8	32.3	30.2	30.9	29.6	26.9	27.1	27.1	27.5	28.1	22	3.95
5	24	0.90	27.9	27.2	36.5	33.2	34.4	32.1	27.3	27.2	27.2	27.6	28.5	24	4.92
5	26	1	29.2	28.4	40.9	37.2	39.3	37.1	26.9	27.1	27.3	27.9	30	26	4.03
5	30	1.14	34.1	33.8	50.8	46.6	48.9	46.5	27.8	27.4	27.6	28.8	30.1	30	4.21
5	33	1.27	37.5	37.3	56.3	51.2	53.1	49.9	27.8	27.6	27.8	29.2	32.2	33	4.31

TABLE A.14: Specific heat of **Gamma-Aluminium Oxide (0.002%)**

T (min)	V	I	T1	T2	T3	T4	T5	T6	T7	T8	T9	T10	T11	Variac	Specific Heat(Cp)
5	0	-0.01	26	25	28.2	27.2	27.9	26.1	25.2	24.3	25.2	27.2	29	0	
5	22	0.82	26.4	25.4	33.3	30.8	31.9	29.8	25.3	24.6	25.5	27.4	29	22	3.21
5	24	0.90	27.3	26.6	38.5	35.1	36.6	35	25.9	25.1	25.9	27.3	29.1	24	3.15
5	26	0.99	29	29.4	43.2	39.1	40.8	38.2	25.8	25.3	26.2	27.8	30	26	3.31
5	28	1.06	31.8	31.2	48	43.6	45.6	43.4	26.3	25.8	26.4	27.8	30	28	3.42
5	30	1.13	36.2	36.1	54.8	49.9	51.4	48.9	26.4	26.2	26.9	28.8	31.5	30	3.51

TABLE A.15: Specific heat of **Zinc oxide (0.001%)**

T (min)	V	I	T1	T2	T3	T4	T5	T6	T7	T8	T9	T10	T11	Variac	Specific Heat(Cp)
5	0	-0.01	27	25.8	30.6	28.5	297	27.3	27.5	27.8	27.9	28.5	30.5	0	
5	22	0.83	27.6	26.6	34.8	31.8	33.5	31.6	27.8	27.9	28.2	28.8	30.5	22	3.23
5	24	0.91	29.3	28.4	39.9	36.1	37.9	35.2	27.9	28	28.3	29.1	30.9	24	3.63
5	28	1.07	33.4	33	48.8	44.2	46.2	43	28.2	28.4	28.6	29.5	31.2	28	3.71
5	30	1.13	34.3	33.8	50.9	46.8	48.9	46.2	28.5	28.8	28.9	29.9	32	30	3.16
5	33	1.25	39.2	38.8	56.9	52.6	55.1	51.4	29.2	29.1	30.9	30.5	33	33	3.8

TABLE A.16: Specific heat of **Zinc oxide (0.002%)**

T (min)	V	I	T1	T2	T3	T4	T5	T6	T7	T8	T9	T10	T11	Variac	Specific Heat(Cp)
5	0	-0.01	26.6	25.1	30.6	30.1	30.9	28.8	22.9	27.8	25.9	25.8	29.5	0	
5	24	0.92	28.3	27.5	39.6	36.8	37.9	35.5	23	27.9	26.1	25.4	29.6	24	3.46
5	26	0.98	31	30.9	46.1	42.1	44.4	41.5	23.6	28.3	26.3	25.4	29.8	26	3.61
5	29	1.09	33.1	33.1	49.9	45.2	46.9	43.9	24.1	28.3	26.3	25.6	31	29	4.03
5	30	1.14	34	33.1	49.9	50	47.9	44.9	26.1	29.5	27.3	27.3	32	30	4.12

TABLE A.17: Specific heat of **Zinc oxide (0.005%)**

T (min)	V	I	T1	T2	T3	T4	T5	T6	T7	T8	T9	T10	T11	Variac	Specific Heat(Cp)
5	0	-0.01	24.2	22.2	29	26.1	26.6	25.8	26.2	26.7	27.1	28.6	30	0	
5	22	0.82	24.6	22.3	33.9	29.2	30.9	30.8	26.6	26.9	27.5	28.7	30	22	2.98
5	24	0.91	25.9	24	40.1	34.6	36.3	35.2	26.8	27	27.5	28.7	30	24	3.08
5	28	1.06	27	24.9	43.6	37.9	39.9	39.2	27.2	27.3	27.8	28.9	30	28	3.12
5	30	1.13	29.8	27	48.3	42	44.1	41.9	27.2	27.4	28	29	30	30	3.21
5	33	1.24	32.2	29.2	53.6	47.9	50.8	48.9	27.3	27.8	28	29.3	31	33	4.08

TABLE A.18: Specific heat of **Silver (1.38%)**

T (min)	V	I	T1	T2	T3	T4	T5	T6	T7	T8	T9	T10	T11	Variac	Specific Heat(Cp)
5	0	0.03	29.2	27.9	30	29	29.9	27.5	30.8	30.8	30.9	31.3	33	0	
5	22	0.98	29.8	28.8	36	32.8	34.1	32.2	30.8	31.3	30.9	31.3	33	22	3.75
5	24	1.05	30.3	29.3	38	35	36.6	34.8	31.1	31.2	30.9	31	33	24	4.11
5	26	1.13	33.4	32.4	43.1	40	40	38.6	31.2	30.9	31	31.7	33.5	26	4.52
5	30	1.24	35.4	34.8	48.8	44.5	46.8	44.1	31	31.4	31.5	31.3	34	30	4.64
5	33	1.37	39.3	38.4	54.4	49.4	51.5	48.1	31	31.6	31	31.9	34.1	33	3.75

List of Symbols

A : Coulomb constant ($9 \times 10^{9} Nm^2 C^{-2}$

a : Cross section area (m^2)

C : Specific heat (J/kg K)

d : Particle diameter (m/nm)

h : Length of wire (m)

i : Time (Sec)

I : Current

K : Thermal conductivity (W/mK)

K_B : Boltzmann constant (1.3807×10^{-23} J/K)

L : Average distance for a particle to travel along one direction due to the particle Brownian motion (m)

l : mean free path (nm)

u : Molecular number density

n : particle concentration (m^{-3})

P : Input power (Watt)

P : Probability for a particle to travel along any direction

Q : Heat flux(W/m^2)

q : electric charge (C)

Pr : Prandtl number

Re : Reynolds number

r : Particle radius (nm)

T : Temperature (K)

ΔT : Temperature diffrence

m : mass (Kg)

V : Voltage (V)

Greek symbols

Φ : Volume fraction of nanoparticles

α : Thermal diffusivity (m^2/sec)

κ : Ratio of thermal conductivity of particle to that of base fluid

ρ : density (kg/m^3)

γ : Ratio of nanolayer thickness to radius of nanoparticles

μ : Viscosity (Pa.s)

ν : Kinematic viscosity (Stoke)

Δ : Nanolayer/interfacial layer thickness (nm)

χ : Shape factor

ω : Weight fraction (%)

T : Temperature in K

D :Diameter in nm

μ :Viscosity in pascalsec

ρ_f :Density of base fluid

ρ_P :Density of particle

C_{P_P} :Specific heat of particle in KJ/KgK

C_{P_f} :Specific heat of particle in KJ/KgK

Subscript

g : Glass spacers

p : Particle/nanoparticle

f : Base fluid

l : Liquid phase (for base fluid)

nf : Nanofluid

EDL : Electrical double layer

Abbreviation

DI : Deionized water

R : Correlation coefficient

Cpnf : specific heat of the nanofluid

Cps : specific heat of the solid nanoparticle

□ : particle volumetric concentration

Cpbf : specific heat of the base fluid.

REFERENCES

Choi S. U. S., 1999, Nanofluid Technology: Current Status and Future Research, Stephen U.S. Choi Energy Technology Division Argonne National Laboratory Argonne, Il 60439.

.

Chon C.H, Kihm K.D., Lee S.P. and Choi S.U.S., 2005 : Empirical Correlation Finding The Role of Temperature and Particle Size for Nanofluid (Al_2O_3) Thermal Conductivity Enhancement, Physics Letter, Vol. 87, Issue. 153107, PP. 1-3.

Choi U.S Stephen, Wang H.P., 1995 : Enhancing thermal conductivity of fluids with nanoparticles, Siginer D.A., Developments and Applications of Non-Newtonian Flows, FED-vol. 231/MD-vol. 66, ASME, New York, pp. 99–105.

Chandrasekar M, Suresh S and Bose A.C, 2010 :Experimental investigations and theoretical determination of thermal conductivity and viscosity of al2o3/water nanofluid, J. Experimental Thermal and Fluid Science 34 (2010) 210-216.

Cristina Buzea, Ivan Pacheco and Kevin Robbie, 2007: Nanomaterials and Nanoparticles: Sources and Toxicity, Biointerphases, Vol 2, pp. 17-71.

Das S.K., Putra N., Thiesen P. and Roetzel W., 2003: Temperature Dependence of Thermal Conductivity Enhancement for Nanofluids, Heat Transfer, Vol. 125, PP. 567-574.

D. Zhu, X. Li, N. Wang, X. Wang, J. Gao and H. Li, 2009 : Dispersion behavior and thermal conductivity characteristics of Al_2O_3–H_2O nanofluids, Applied Physics, 9 131–139.

Das S.K, Choi S.U.S., W. Yu and K. Pradeep, 2008 : Nanofluids Science and Technology, Wiley Interscience. Applied Physics, 9 131–139.

Echlin. P, Handbook of sample preparation for scanning electron microscopy and X-Ray Microanalysis, DOI: 10.1007/978-0-387-85731-2_12.

Eastman J.A., Choi U.S Stephen, Li S., Thompson L.J., (1997), Enhanced thermal conductivity through the development of nanofluids, Proceedings of the Symposium on Nanophase and Nanocomposite Materials II, vol. 457, Materials Research Society, USA, pp. 3–11.

J. Buongiorno, (2006)"Convective transport in nanofluids," Journal of Heat Transfer, vol. 128, no. 3, pp. 240–250, 2006.

P. Bhattacharya, A.N. Samanta and S. Chakraborty(2009),: Numerical study of conjugate heat transfer in rectangular microchannel heat sink with Al_2O_3/H_2O nanofluids, J. Heat Mass Transfer 45 1323–1333.

Gallego M.J.P, Lugo L, Legido J.L and Pineiro M.M :Thermal conductivity and viscosity measurements of ethylene glycol-based Al_2O_3 nanofluids, Nanoscale Research Letters 6 (211) (2008) 1-11.

Incropera, F. P., and DeWitt, D. P., 1996, Introduction to Heat Transfer, 3rd edition., Wiley, New York.

Khanafer. K and Vafai.K : A critical synthesis of thermophysical characteristics of nanofluids, Int. J. Heat and Mass Transfer 54 (2011) 4410-4428.

Mintsa H.A., Roy G. and Nguyen C.T., 2007 : New Temperature Dependent Thermal Conductivity Data of Water Based Nanofluids, 5th IASME/WSEAS Int. Conference on Heat Transfer, Thermal Engineering and Environment, Athens, Greece, PP. 290-294.

Murshed S.M.S., Leong K.C. and Yang C., 2005 : Enhanced thermal conductivity of TiO2—water based nanofluids, International Journal of Thermal Sciences, Vol. 44, PP. 367–373.

S. Q. Zhou and R. Ni, :"Measurement of the specific heat capacity of water-based Al2O3 nanofluid," Applied Physics Letters, vol. 92, Article ID 093123, 3 pages, 2008.

Swanson E.J., Tavares J, Coulombe.S : Improved dual-plasma process for the synthesis of coated or functionalized metal nanoparticles, IEEE Trans. Plasma Sci. 36 (4) (2008) 886–887.

S. Q. Zhou and R. Ni, (2008) : "Measurement of the specific heat capacity of water-based Al2O3 nanofluid," Applied Physics Letters, vol. 92, no. 9, Article ID 093123, 2008.

Serrano E, Rus G, Martínez JG. Nanotechnology for sustainable energy. Renew Sust Energy Rev 2009;13(December (9)):2373–84

The ASHRAE Centennial: 100 Years of Progress", ASHRAE Historical Committee, 1994

Timofeeva E.V., Gavrilov A.N., McCloskey J.M., Tolmachev Y.V., Sprunt S., Lopatina L.M. and Selinger J.V., 2007 : Thermal Conductivity and Particle Agglomeration In Alumina Nanofluids: Experiment And Theory, Physical Review E, Vol. 76, Issue. 061703, PP. 1-16.

U. Rea, M. McKrell, L.W. Hu and J. Buongiorno(2009) : Laminar convective heat transfer and viscous pressure loss of alumina–water and zirconia–water nanofluids, Int. J. Heat and Mass Transfer 52 2042–2048.

Wang Z. L., Tang D.W., Liu S., Zheng X. H., Araki N., 2007 : Thermal-Conductivity and Thermal-Diffusivity Measurements of Nanofluids by 3ω Method and Mechanism Analysis of Heat Transport, Thermophys, Vol. 28, PP. 1255–1268.

Xie H.Q, Wang J.C, Xi T.G, Liu Y , Ai F and Wu Q.R, Thermal conductivity enhancement of suspensions containing nanosized alumia particles, Applied Physics 91 (7) (2002) 4568-4572.